

Decoherence-induced self-dual criticality in topological states of matter

Qingyuan Wang,¹ Romain Vasseur,^{2,3} Simon Trebst,⁴ Andreas W.W. Ludwig,⁵ and Guo-Yi Zhu^{1,*}

¹The Hong Kong University of Science and Technology (Guangzhou), Nansha, Guangzhou, 511400, Guangdong, China

²Department of Theoretical Physics, University of Geneva, 24 quai Ernest-Ansermet, 1211 Genève, Switzerland

³Department of Physics, University of Massachusetts, Amherst, MA 01003, USA

⁴Institute for Theoretical Physics, University of Cologne, Zùlpicher Straße 77, 50937 Cologne, Germany

⁵Department of Physics, University of California, Santa Barbara, California 93106, USA

(Dated: February 21, 2025)

Quantum measurements can be employed to induce decoherence in a restricted segment of a larger quantum many-body state, while simultaneously engineering long-range entanglement for its remaining constituents. Though this two-fold character of measurements in open quantum systems has been appreciated, e.g., in the context of state preparation, a deeper conceptual understanding is called for, particularly with regard to symmetry as an organizing principle for such entangled states of matter. Here we discuss the role of *self-dual symmetry* – a fundamental notion in theoretical physics – in mixed states, showing that the decoherence of electric (e) and magnetic (m) vortices from the 2D bulk of the toric code, or equivalently, a 2D cluster state with symmetry-protected topological order, can leave a (1+1)D *quantum critical mixed state* on the boundary protected by a weak Kramers-Wannier self-dual symmetry. The corresponding self-dual critical bulk is described by the $N \rightarrow 1$ limit of the 2D Non-linear Sigma Model in symmetry class D at Θ -angle π , with target space $SO(2N)/U(N)$. We establish that this is a “measurement-version” of the *Cho-Fisher model* in which uncorrelated quenched disorder is replaced by the intrinsic randomness of Born measurement outcomes, resulting in distinct universal critical properties some of which we obtain numerically (and the known absence of a Majorana metal). An explicit breaking of the self-duality, by incoherent noise amounting to fermion interactions or (non-interacting) coherent deformation, is shown to induce an RG crossover from this self-dual critical state to Nishimori criticality or to it from a novel type of “Ising+ criticality”, respectively, both of which are related to the random-bond Ising model in different replica limits and are described by non-unitary conformal field theories of non-interacting fermions, as is the self-dual point. Using an unbiased numerical approach combining tensor network, Monte Carlo, and Gaussian fermion simulations, we chart out a global phase diagram as witnessed by coherent information and entanglement entropy measures. On a conceptual level, our protocol can be viewed as a non-unitary extension of the measurement-based quantum computation scheme that results in an imaginary-time evolved quantum Ising chain, subjected to measurement-induced randomness. Our results point a way towards a general understanding of mixed-state criticality in open quantum systems in terms of symmetry and topology, while also providing a concrete protocol amenable to simulation on near-term quantum devices.

Since the early days of quantum mechanics, Born’s rule has been providing a link connecting quantum measurements to the probabilistic dynamics they induce. Its generalization from few-body to many-body quantum systems allows to connect quantum many-body dynamics to (classical) statistical mechanics with strong disorder. A well-studied example of this link is the connection of noisy topological quantum memories [1] to the random bond Ising model (RBIM) and the emergence of an error threshold described by Nishimori criticality [2] as the disorder-induced generalization of Ising criticality. Such a link to Nishimori physics has recently been uncovered also in the context of monitored quantum circuit dynamics [3–5], many-body teleportation thresholds [6], and mixed-state phase transitions in open quantum systems [7–9]. From a symmetry perspective, the most striking difference between clean Ising and disordered Nishimori criticality is their relation to Kramers-Wannier *self-duality* [10], which is an idiosyncratic symmetry for the clean Ising transition, while for Nishimori criticality it is inevitably and strongly broken [11, 12]. Self-duality has long been appreciated as one of the most elegant symmetries for a many-body system to exhibit, often serving as a guiding light to deeper under-

standing, such as Wegner’s seminal insight [13] connecting spin to gauge-invariant models and, subsequently, the interplay of gauge and matter shaped by t’Hooft [14], and the Fradkin/Shenker phase diagram [15]. Today, self-duality is again providing a spotlight in the exploration of quantum circuits where its non-invertible algebraic character, its relation to anomalies and fractionalization are broadly discussed [16–25]. This has led us to question whether in the context of *monitored* circuit dynamics there is a way to twist Born’s rule into preserving self-duality, what kind of criticality this might induce, and how decoherence or coherent deformations might then break it down, e.g., to Nishimori criticality.

In this manuscript, we show that self-duality can naturally appear (even at zero temperature) in the form of an average “weak” symmetry [26–28] when decohering (i) a short-range entangled symmetry protected topological state (SPT [29]), (ii) a long-range entangled toric code [30], or (iii) a measurement prepared cat state [3, 31], either by projective measurement or by maximal dephasing noise. Specifically, we demonstrate that the *bulk* decoherence of a cluster state [32–35], which on a Lieb lattice exhibits $Z_2^{(0)} \times Z_2^{(1)}$ (0-form and 1-form) SPT [36–39], can lead to a mixed quantum critical state *on its boundary*, described by a self-dual random bond Ising model. The same boundary state can appear upon decohering a toric code or a mixed Greenberger-Horne-Zeilinger

* guoyizhu@hkust-gz.edu.cn

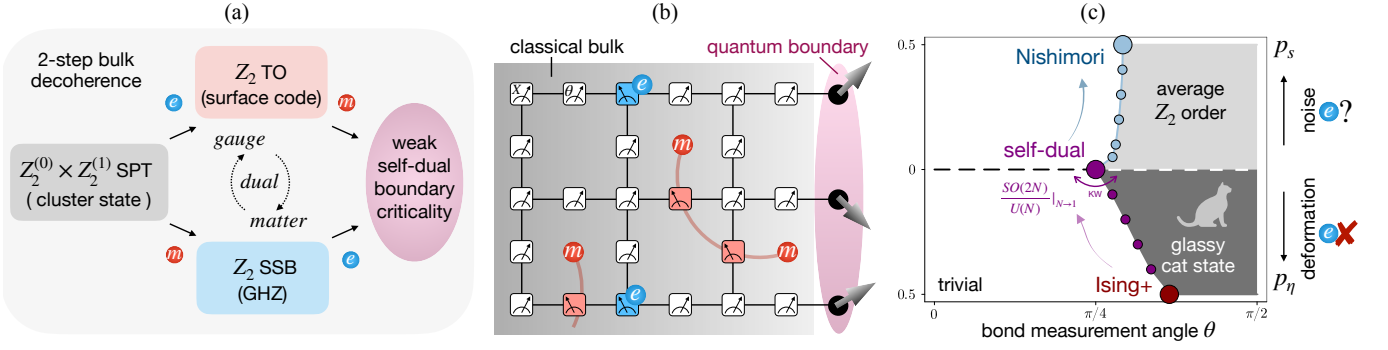


FIG. 1. **Decoherence schematic, circuit protocol, and phase diagram.** (a) Schematic of the setup: a $Z_2^{(0)} \times Z_2^{(1)}$ SPT can be realized as a cluster state on a Lieb lattice (with site and bond qubits), which can be viewed as a lattice gauge state with matter electric charge e - and gauge magnetic flux m -vortices, that are dual to each other. Dephasing the site qubit uncondenses e resulting in average or correctable topological order as a deconfined gauge state that spontaneously breaks the 1-form $Z_2^{(1)}$ symmetry. Dephasing the bond qubit uncondenses m and leads to the GHZ-like state as an average $Z_2^{(0)}$ spontaneous symmetry breaking order. When both e and m are uncondensed, it can leave a boundary critical state with weak self-dual symmetry and weak $Z_2^{(0)}$ symmetry. (b) Protocol: preparing a cluster state on a Lieb lattice, and measure the site qubit in X basis, and the bond qubit in $\cos(\theta)Z + \sin(\theta)X$ basis with a tunable angle θ , leaving a boundary chain untouched. The bulk can also be viewed as a “register” that records all the measurement outcomes. In the schematic, we deduce the e and m -vortices from the measurement outcomes. (c) The phase diagram. When the bond measurement angle θ is tuned to the symmetric angle $\pi/4$, the system exhibits the weak self-dual criticality, described by the $SO(2N)/U(N)$ Non-linear Sigma Model (NLSM) at topological Θ -angle π in $N \rightarrow 1$ limit. Changing the measurement angle θ at the microscopic level has the same effect as changing the topological Θ -angle in the long-wave-length theory. Different perturbations can be used to tune the e -vortices away from duality: the upper panel uses the (measurement) noise to mask and blur the existence of an e -vortex, while the lower panel uses the deformation to damp it. Within the phase diagram, the white region is the trivial state; the dark gray region indicates the strong-to-weak spontaneous-symmetry-breaking (SW-SSB) of Z_2 ordered phase with long-range glassy correlation $[\langle Z_i Z_j \rangle] \neq 0$ and $[\langle Z_i Z_j \rangle] = 0$ (easily verified at $\theta = \pi/2$); the light gray region has only weak Z_2 symmetry due to the noise, but exhibits the same long-range correlation. There are 3 paradigmatic critical points in this phase diagram: the Nishimori critical point, the weak self-dual critical point, and the Ising+ critical point. The arrows in the phase diagram outline the RG flow indicated by our numerical results. Here we unfold the two perpendicular phase diagrams (by tuning p_s and p_η , respectively) into the plane, and their crossing line $p_s = 0 = p_\eta$ is not a phase transition generically.

(GHZ [31]) state (dubbed “Nishimori’s cat” state in Refs. 3 and 5). This trio of states is, of course, not incidental as all three of them – the cluster state on a Lieb lattice, the toric code on one of its sublattices, and the GHZ/cat state on the other sublattice – can be unified via a Z_2 lattice gauge theory [13, 15, 36, 40, 41], where the site and bond qubits in the underlying Lieb lattice are interpreted as matter and Z_2 gauge fields, respectively. When the matter field is decohered in a first step, one obtains a deconfined gauge theory as an intermediate state, which is the topological toric code [30], see Fig. 1(a). If, on the other hand, the gauge field is first decohered, then one obtains a gauge-symmetrized Z_2 ferromagnetic order, i.e. the state dubbed Nishimori’s cat [3]. Finally, if both the matter and the gauge degrees of freedom are decohered in the bulk, one might naively expect a trivial state. However, the emergence of self-dual symmetry prohibits triviality and protects criticality: a vestigial quantum critical state persists at the boundary – this is the aforementioned critical boundary state that reveals itself upon close inspection of the mixed-state ensemble after bulk decoherence.

From a symmetry perspective, the boundary state inherits the *strong* Z_2 symmetry from the bulk

$$\left(\prod_j X_j \right) \rho = \rho.$$

However, a strong KW self-dual symmetry, $\text{KW}\rho \propto \rho$, is

explicitly broken by the measurement-induced disorder in the bulk. Nevertheless, a *weak* KW self-dual symmetry

$$\text{KW} \rho \text{KW} = \rho$$

can be preserved on average, which can protect the mixed critical state, forbidding a flow into the trivial state or a strong-to-weak spontaneous symmetry breaking phase [8, 9] with spin glass order parameter [3, 5].

Before going into the details of our study, we want to provide a brief overview of our main findings. Fig. 1 summarizes the conceptual idea of decohering the SPT order of a cluster state via the quantum circuit schematically illustrated in panel (b). Introducing both incoherent noise (parametrized by p_s) and a coherent deformation (parameterized by p_η) we have explored the phase diagram of panel (c), which centers around a line where self-duality is preserved as a weak symmetry (parametrized by the measurement angle θ for $p_s = p_\eta = 0$) and which exhibits a critical point whose universality and field theoretical description is distinct from both the Nishimori criticality induced by incoherent noise and yet another type of critical behavior, dubbed “Ising+” induced by the coherent deformation – both of which break the weak self-duality along the center line of our phase diagram.

Using extensive numerical simulations that combine elements from tensor network, Gaussian fermion, and Monte Carlo sampling, we estimate the critical exponents of this

TABLE I. **Overview of the mixed-state criticality originating from Ising.** Shown is a characterization of the three mixed-state critical theories of the phase diagram in Fig. 2(c), and a comparison to the pure-state Ising universality class. The asterisk indicates results with system size $L_x > 1000$ taken from Ref. 42. Critical exponents: $c_{\text{ent}}^{\text{vN}}$ and $c_{\text{ent}}^{(\infty)}$ characterize the scaling dimensions of the boundary condition changing operators that govern the Born-averaged von Neumann and the ∞ -Rényi entanglement entropies of the boundary 1+1D quantum states. c_{Casimir} is the effective central charge that governs the Shannon entropy density of the 2D bulk. Δ_m is the typical m -vortex scaling dimension that governs the change of the bulk entropy upon changing the boundary condition.

| criticality | Nishimori | weak self-dual | Ising+ | Ising |
|------------------------------|------------------|---------------------|--------------------|---------|
| 1D quantum | mixed | mixed | mixed | pure |
| self-dual symmetry | broken | weak | broken | strong |
| 2D stat mech | disordered | disordered | disordered | clean |
| disorder probability | $\mathcal{Z}(m)$ | $\mathcal{Z}(em)^2$ | $\mathcal{Z}(m)^2$ | 0 |
| ν | 1.52(2)* | 1.72(8) | 1.00(5) | 1 |
| conformal symmetry | non-unitary | non-unitary | non-unitary | unitary |
| central charge | 0 ^a | 0 | 0 | 1/2 |
| $c_{\text{ent}}^{\text{vN}}$ | 0.410(1)* | 0.795(1) | 0.310(2) | 1/2 |
| $c_{\text{ent}}^{(\infty)}$ | — | 0.484(1) | — | 1/4 |
| c_{Casimir} | 0.464(4)* | 0.437(7) | — | 1/2 |
| Δ_m | 0.341(1)* | 0.259(1) | — | 1/8 |

^a See Sec. III B for a discussion of the definition of the free energy.

novel self-dual quantum critical point as well as the other two critical theories, relying primarily on Shannon entropy, entanglement entropy, and coherent information measures. A summary of the three types of criticality is given above in Table I. Having established that these three critical theories fall into distinct universality classes, we explore the renormalization group (RG) flow between them by tracking the changes of critical exponent and central charge estimates as we break the self-dual symmetry upon moving away from the center line of our phase diagram. Notably, we find clear numerical evidence that incoherent noise initiates an RG flow from self-dual to Nishimori criticality. On the other hand, upon introducing a coherent wave function deformation that breaks the self-duality, we discover another critical theory (in the limit of infinitely strong deformation) that analytically can be described by a non-unitary conformal field theory (CFT), which retains the unitary Ising CFT in a subset of its operators, which is why we have dubbed it “Ising+” criticality. In our phase diagram, we find that this critical point is an unstable fixed point with numerical evidence for an RG flow back to the weak self-dual criticality (Table I).

The remainder of this manuscript provides a detailed account of this physics, with Sec. II introducing our mixed-state preparation protocol and its decoherence channels. We also briefly point out the underlying Z_2 gauge symmetry and

its tensor network representation. In Sec. III we then proceed to introduce four alternative model representations in terms of a (1+1)D monitored circuit, a 2D classical stat mech model, followed by a (1+1)D Majorana circuit and a (2+1)D Chalker-Coddington network model, along with a discussion of Kramers-Wannier self-duality in all four formulations. The self-dual critical state is discussed in detail in Sec. IV based on its coherent information, bulk Shannon entropy, and boundary entanglement entropy. In Sec. V we then discuss the entire phase diagram of Fig. 1(c) in detail with a particular emphasis on the RG flows between the various critical theories. We close with a broader discussion and an outlook in Sec. VI.

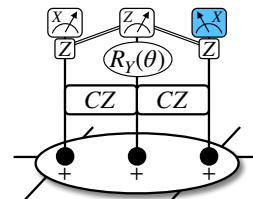
II. MODEL

A. Protocol: preparation and decoherence

Our protocol comprises two principal steps: (i) the preparation of an entangled resource state – the cluster state, which, in step (ii), is subject to decoherence by either projective measurements or 50% Pauli noise in some orientable basis direction. For the first step we prepare a short-ranged entangled cluster state [32]: $\prod CZ |+\rangle^{\otimes N}$ using a finite-depth circuit on a (square) Lieb lattice as illustrated in Fig. 1(b), where we discriminate between the bond qubits Z_{ij} and the site qubits Z_j with $i(j)$ denoting sites of the square lattice. Secondly, we dephase all the qubits in the bulk in a designated basis, by projectively measuring the site qubits in the X direction and the bond qubits in a tilted direction

$$\sigma^\theta = \cos(\theta)Z + \sin(\theta)X.$$

The “measurement angle” θ can also be understood as the angle of a coherent unitary rotation error around the Y -axis right before a measurement in the Z -basis [3, 4, 43] (not to be confused with the topological Θ -angle of the NLSM). Schematically, an elementary building block of this circuit for a given bond then takes the form



Here the qubits are originally initialized in X -basis eigenstates $|+\rangle = X|+\rangle$, then subjected to a controlled- Z (CZ) gate $CZ = \text{diag}(1, 1, 1, -1)$ that (maximally) entangles the two neighboring qubits into a cluster state. Before the final round of measurements in the X and Z bases, respectively, the bond qubit is rotated via $R_Y(\theta) = \exp(i\theta Y/2)$ by the measurement angle θ . The measurement channel can be viewed as a maximally dephasing channel: $\mathcal{N} = \mathcal{N}_s \circ \mathcal{N}_b$ where $\mathcal{N}_s(\cdot) = (\cdot) + X(\cdot)X$ acts on the site qubits and $\mathcal{N}_b(\cdot) = (\cdot) + \sigma^\theta(\cdot)\sigma^\theta$ acts upon the bond qubits. If the measurement outcome on a bond is negative $Z_{ij} = -1$, we perform a feedback $Z_i Z_j$ to its

adjacent site qubits, which equivalently flips the site measurement outcome and can be done in a post-processing manner. Note that, from a symmetry perspective, there is a distinction of the site versus bond qubits – the SPT order of the cluster state on the underlying Lieb lattice is protected by a 0-form Z_2 symmetry for the site qubits and a 1-form magnetic $Z_2^{(1)}$ symmetry for the bond qubits [36]. Due to this inequivalence of the symmetry forms, the decoherence of the site and the bond qubits $\mathcal{N}_s \circ \mathcal{N}_b$ leads to two distinct intermediate states when decomposing it into two steps:

- (i) \mathcal{N}_b : If first the bond qubits are measured and de-phased [3, 4], this leaves a 2D state which can be tuned between a product state and the “Nishimori cat” state [3], i.e. a glassy GHZ state exhibiting strong-to-weak spontaneous symmetry breaking (SW-SSB) order [8, 9] [44]. This state can also be viewed as a randomized version of a Rokhsar-Kivelson state [45–47], which can be cast as a 2D projected entangled pair state (PEPS) [48].
- (ii) \mathcal{N}_s : If the site qubits are measured first instead, this leaves a 2D toric code with e anyons at random but known locations, as eigenstates of the toric code Hamiltonian [49]. Therefore one can apply conditional Pauli string operators to pair up and remove the e anyons to correct any post-measurement state into the clean toric code [50–52]. The toric code is then subjected to a coherent “error” – a unitary rotation by $R_Y(\theta) = \exp(iY\theta/2)$ on the bond qubits [6, 53–60], which preserves the electric-magnetic self-duality of the toric code [61–65] for $\theta = \pi/4$.

Given these two routes through distinct intermediate states, the final state of our protocol can be equally interpreted as the vestigial boundary *quantum* state after the bulk decoherence of a cluster state with $Z_2^{(0)} \times Z_2^{(1)}$ SPT, a Nishimori cat state with SW-SSB, or a toric code with topological order.

B. Z_2 gauge perspective for the intermediate state

For our later discussion it is useful to connect the states prepared by our protocol to the fundamental physics of a Z_2 gauge theory [40]. To do so, let us start by noting that the cluster state on the Lieb lattice satisfies the following two sets of stabilizers

$$\begin{array}{c} \textcircled{Z} \\ | \\ \textcircled{X} \\ | \\ \textcircled{Z} \end{array} = 1, \quad \begin{array}{c} | \\ \textcircled{Z} \\ | \\ \textcircled{X} \\ | \\ \textcircled{Z} \end{array} = 1, \quad (1)$$

for the site and the bond qubits of the square lattice, respectively. The vertex stabilizers can be interpreted as a Z_2 Gauss law, where $|X_j = -1\rangle$ for the site qubit denotes a Z_2 *matter charge* usually labeled as e -vortex, and Z_{ij} operator for the bond qubit denotes a corresponding electric field. Consequently, $|X_{ij} = -1\rangle$ labels a nonzero gauge field, and the bond

stabilizer $Z_i X_{ij} Z_j = 1$ describes the minimal coupling between matter and charge, where the matter hopping is coupled with the gauge connection X_{ij} operator [40]. When the matter charge hops around a plaquette, it picks up a negative sign factor if the Wilson loop $\prod_{(ij) \in \square} X_{ij} = -1$, which is usually dubbed an m -vortex, denoting a *magnetic vortex*.

When one projectively measures the matter qubit in the X basis, the matter charge is frozen into a classical configuration, leaving the bond qubits to form a pure gauge theory with random background charges but free of magnetic vortices. This is a random topological toric code state, see the top path in Fig. 1(a). When one instead projectively measures the gauge qubit in a tilted basis, it is the gauge field that is quenched, leaving the site qubits as matter degrees of freedom forming a Nishimori’s cat state [3].

C. Tensor network state representation

We can label the bulk classical bits after measurement in the following way: $e_j = 0(1)$ if the site qubit at site j is measured to be $X_j = \pm 1$ (after absorbing the Z conditioned upon the adjacent bond qubit measurement outcomes); if the bond qubits at the center of the bond between site i and j are measured (after having been rotated by an angle θ) to be $Z_{ij} = -1$, we associate that with an m string crossing the bond, and the end point of a string with $Z_{ij} = -1$ all along the way is denoted by an m -vortex, $m_p = 1$ (where p denotes the plaquette).

This post-measurement state exhibits, at its boundary, a 1D quantum state $|\psi(em)\rangle$, which can be represented as an *exact* tensor network state of the form

$$|\psi(em)\rangle = \begin{array}{c} \vdots \\ \begin{array}{cccc} \textcircled{\cdot} & \textcircled{\cdot} & \textcircled{\cdot} & \textcircled{\cdot} \\ | & | & | & | \\ \textcircled{\cdot} & \textcircled{\cdot} & \textcircled{\cdot} & \textcircled{\cdot} \\ | & | & | & | \\ \textcircled{\cdot} & \textcircled{\cdot} & \textcircled{\cdot} & \textcircled{\cdot} \\ | & | & | & | \\ \textcircled{\cdot} & \textcircled{\cdot} & \textcircled{\cdot} & \textcircled{\cdot} \\ | & | & | & | \\ \textcircled{\cdot} & \textcircled{\cdot} & \textcircled{\cdot} & \textcircled{\cdot} \\ \vdots & \vdots & \vdots & \vdots \end{array} \\ \vdots \end{array} = \dots \quad (1)$$

where each node at the vertex is a diagonal delta tensor, and each box on the bond is a 2-by-2 matrix $e^{\beta/2} + e^{-\beta/2} X$, with $\tanh \beta = \sin \theta$. A negative measurement outcome on the bond qubit injects an X to the bond, while a negative measurement outcome on the site qubit injects a Z to the vertex. Note that this tensor network state is un-normalized, since its norm $P(em) = \langle \psi(em) | \psi(em) \rangle$ captures the measurement probability dictated by Born’s rule.

Because of the underlying Z_2 gauge symmetry, one can fluctuate the m -string across the lattice [3], without altering the post-measurement boundary state. The latter is only determined by the *gauge invariant* m -vortex configuration [1]. This can be explicitly verified by propagating the X -string through the tensor network [66]. Since a gauge transformation can be independently generated by creating a local X loop around any vertex, one can count a total number of $2^{L_x L_y}$ gauge-equivalent configurations that share the same boundary quantum state $|\psi(em)\rangle$. We will therefore label the bulk bits

only by their m -vortex configuration for brevity. The final state can then be compactly written as

$$\rho = \sum_{em} |em\rangle\langle em|_C \otimes |\psi(em)\rangle\langle\psi(em)|_Q, \quad (2)$$

where $|em\rangle$ refers to the classical state of the bulk bits, denoted by C , corresponding to the measurements record. The remaining quantum bits at the boundary are denoted by Q . If the 2D state is placed on a cylinder, i.e. one applies a periodic boundary condition in the vertical direction, then there is one additional (very big) plaquette at the left boundary with L_x number of edges (see Fig. 4a inset for a schematic), where the absence (presence) of an m -vortex labels the even (odd) sector of the mixed state.

D. Symmetries

The state (2) possesses a strong Z_2 Ising symmetry that acts on the qubits on the boundary

$$\left(\prod_{j \in Q} X_j \right) \rho = \rho = \rho \left(\prod_{j \in Q} X_j \right), \quad (3)$$

which will be shown to exhibit a SW-SSB transition by tuning the measurement angle θ . The duality symmetry is inherited from the pre-measurement state, which in the toric code or gauge theory is an electric-magnetic duality [6, 61]

$$\text{KW} : \quad e \leftrightarrow m, \quad \theta \leftrightarrow \pi/2 - \theta, \quad (4)$$

where the operator KW will be explicitly written in the next section. The presence of the KW duality dictates a symmetric critical state at $\theta = \pi/4$, which is invariant under the duality transformation and can be interpreted as the gapless phase of matter protected by such symmetry [16, 23]. Under such a KW transformation, each post-measurement pure state at the boundary is mapped to its duality counterpart

$$\text{KW} |\psi(em; \theta)\rangle = |\psi(me; \pi/2 - \theta)\rangle, \quad (5)$$

which means the presence of em disorder breaks the duality as a strong symmetry for the pure state. Nonetheless, the mixed state that encapsulates all the weighted trajectories are invariant under a *weak* symmetry [26–28] version of the self-duality at $\theta = \pi/4$

$$\text{KW}\rho \neq \rho, \quad \text{KW}\rho\text{KW} = \rho. \quad (6)$$

Note that the weak symmetry of the density matrix is also sometimes referred to as an ‘‘average’’ symmetry common in open quantum systems described by Lindbladian or density matrix [7, 8, 26–28, 67–70]. As its strong symmetry counterpart, the weak self-duality here has the same predictive power: that it maps the SW-SSB phase at $\theta > \pi/4$ to the trivial phase at $\theta < \pi/4$, and thus the mixed quantum state at the self-dual $\theta = \pi/4$ point must remain critical, despite the presence of randomness. Namely, the otherwise *pure* Ising critical state with strong self-duality is turned into an intrinsically *mixed* quantum critical state with weak self-duality.

E. Mixed state dynamics

Finally, note that the object of interest in the following is the total mixed state of the bulk *and* the boundary – we will show that this bulk-boundary mixed state can exhibit long-range entanglement. If, on the contrary, one considers only the boundary mixed state by simply tracing out the bulk (and thereby throwing out all bulk measurement outcomes), the resulting boundary density matrix $\sum_{em} |\psi(em)\rangle\langle\psi(em)| = \mathbb{I}$ is a short-range entangled maximally-mixed state. Such a distinction between monitored dynamics (keeping the measurement outcomes) versus dissipative dynamics (averaging over measurement outcomes) is related to the fact that measurement-induced phase transitions [71, 72] are only visible in the ensemble of quantum trajectories, but not in the associated quantum channel [73, 74]. So it is crucial to keep a record of the measurement outcomes, which in our case are represented by the bulk qubits of the system.

III. EQUIVALENT MODEL REPRESENTATIONS

To understand the unusual phenomenon of our mixed-state criticality and particularly its manifestation in a critical boundary state, we enumerate four distinct, but mathematically equivalent models that all capture this physics: a monitored (1+1)D quantum Ising chain, a 2D disordered classical statistical mechanics model, a monitored (1+1)D Majorana fermion chain, and the (2+1)D Chalker Coddington network model. We discuss the Kramers-Wannier duality in these representations of the problem.

A. (1+1)D monitored quantum circuit

Our first representation follows the spirit of measurement-based quantum computation (MBQC) [75, 76], where one views one spatial dimension of a resource quantum state (prior to any measurement) as a fictitious time dimension and a subsequent sequence of spatial measurements then allows to effectively induce a unitary evolution (which implements a quantum computation) along this fictitious time. Here, in analogy, we can also view one spatial dimension of our bulk quantum state (prior to the measurements) as a fictitious time dimension, which then evolves under measurement and builds up the entanglement in the boundary quantum state (corresponding to the final time). Our circuit protocol, recast as tensor network diagram, can then be derived to be equivalent to a (1+1)D *imaginary-time* evolving transverse-field Ising model. The bulk classical bits serve as the ‘‘register’’ that record the measurement outcomes, which determine the evolution of the quantum state, i.e. its quantum trajectory.

Clean Ising in a uniformly post-selected trajectory

To discuss the physics of our protocol in this representation, let us first consider the post-selected case where all measure-

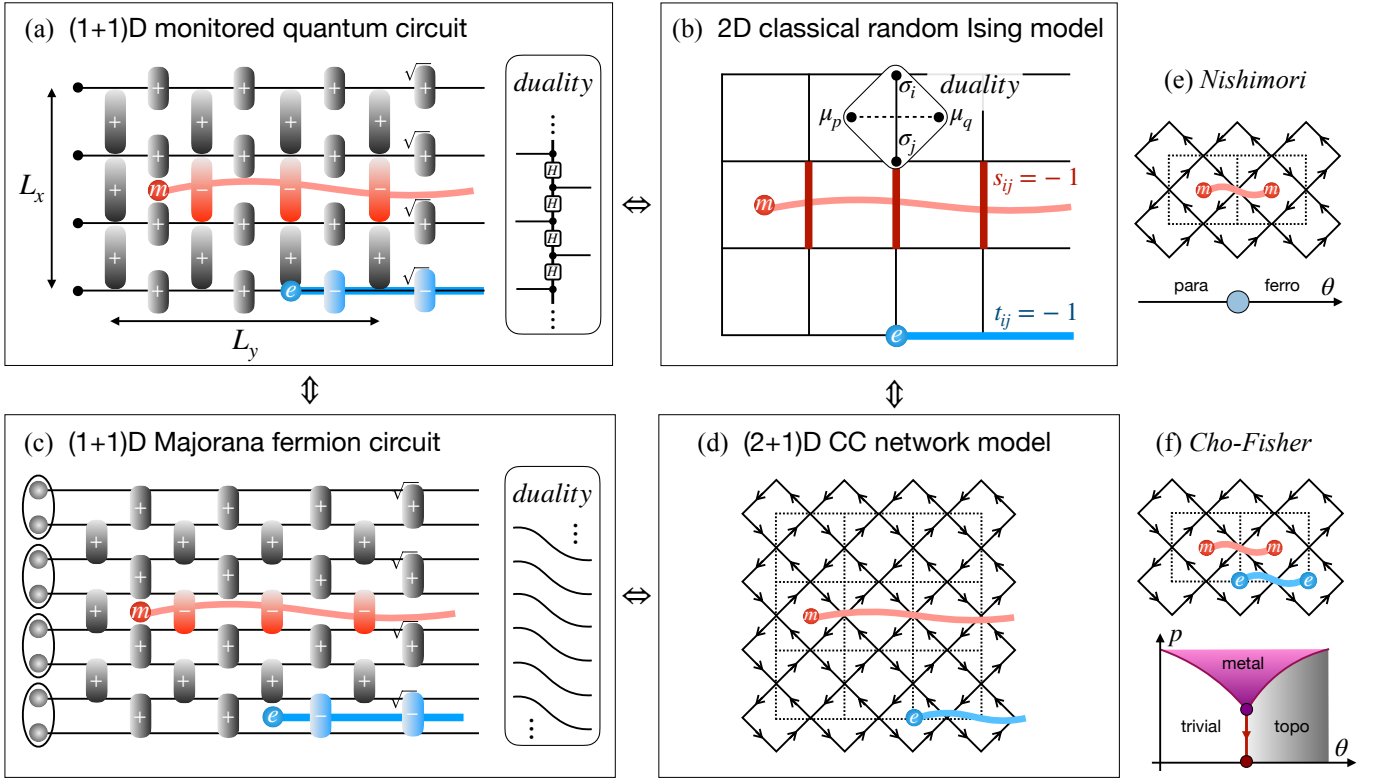


FIG. 2. **Four equivalent model perspectives and their respective duality transformations.** (a) **(1+1)D monitored quantum circuit**, with L_x qubits and circuit depth L_y , where each gate is an imaginary time evolution with random sign. The temporal kink of sign change of the ZZ evolution defines an m -vortex, while that for the X evolution defines an e -vortex. The duality transformation can be expressed in terms of a cluster matrix-product operator (MPO), with Hadamard gate matrix sandwiched by the diagonal delta tensors. (b) **2D classical statistical model** with defect strings pulled by the e and m -vortices. The red defect string runs along the dual lattice and flips the sign of the Ising coupling from ferromagnetic to anti-ferromagnetic coupling, while the blue defect string stretches along the original lattice and inserts an Ising spin operator at the end of the string (the location of the e -vortex) to the Boltzmann weight changing its *sign*. Both strings can fluctuate across the lattice by gauge transformation, and do not change the gauge invariant partition function that is determined only by the e and m locations. The duality transformation replaces the vertex variable σ by the plaquette variable μ . (c) **(1+1)D Majorana quantum circuit**, by Jordan Wigner transforming (a). The duality transformation is a translation of the Majorana lattice. (d) **(2+1)D Chalker Coddington (CC) network model for symmetry class D** . The underlying dashed line illustrates the spin lattice as in (b). The solid lines with arrows denote the fermion propagator, where the vertex denotes the scatterer. There are two representative CC network models: (e) RBIM along Nishimori line that has only the m -vortices, which undergoes the Nishimori transition from a paramagnetic phase to the ferromagnetic phase, as shown schematically; (f) The CF model that has e and m vortices, whose schematic phase diagram comprises a metal phase upon finite vortex density. Despite the equivalence under a fixed vortex configuration, the conventional CF model takes $N \rightarrow 0$ replica limit which is fundamentally distinct from our case where the $N \rightarrow 1$ replica limit is taken.

ment outcomes are positive. By viewing each column slice of the network as a time step, the evolution, schematically illustrated in Fig. 2(a), is generated by the following non-unitary transfer operator

$$M = \sqrt{M_X} M_Z \sqrt{M_X}, \quad M_X = e^{\frac{\beta'}{2} \sum_j X_j}, \quad M_Z = e^{\frac{\beta}{2} \sum_j Z_j Z_{j+1}},$$

as an imaginary-time evolution of the transverse-field Ising model, with $\tanh \beta = \sin \theta$ and $\tanh \beta' = \cos \theta$. Note that the square root of M_X is necessary to maintain the Hermitian [77] property of the transfer matrix M . This transfer matrix evolution is rigorously a discrete brickwall circuit, *without* any Trotterization approximation.

The KW duality transformation operator can be written as

a cluster MPO [20, 78, 79] in the Fig. 2(a), which transforms

$$\text{KW} : \quad Z_j Z_{j+1} \rightarrow X_{j+1/2}, \quad X_j \rightarrow Z_{j-1/2} Z_{j+1/2}.$$

It is equivalent to $\theta \leftrightarrow \pi/2 - \theta$ or $\beta \leftrightarrow \beta'$, which are indeed related by the KW dual relation [10]: $\tanh(\beta'/2) = \exp(-\beta)$. At $\theta = \pi/4$, $\beta = \ln(1 + \sqrt{2}) = \beta'$, the model is (KW) self-dual and the 1D quantum state evolves towards the ground state of the clean critical Ising model, with linear depth of the (1+1)D circuit i.e. $L_y = O(L_x)$. In the absence of e and m random vortices, such a pure state has the *strong* KW self-dual symmetry. That is, in the long wavelength limit, the resulting critical (boundary) state is effectively described by the 2D Ising CFT, protected by the strong Z_2 symmetry and the KW self-dual symmetry. The non-invertibility [17, 21] of the transformation can be deduced when the MPO in Fig. 2(a) is

closed in periodic boundary condition, which inevitably maps $\prod_j X_{j+1/2} = 1$ and thus carries a global parity projector.

Notably, the transfer operators M_Z and M_X above are non-unitary operators, which can be interpreted as the Kraus operators of effectively *weak* measurements of the $Z_j Z_{j+1}$ and X_j operators in the (1 + 1)D dynamics. Note that these tunable effective weak measurements should not be confused with the projective measurements of the 2D bulk.

Measurement-induced random trajectories

Due to the uncertainty principle and the probabilistic nature of quantum measurement, our effective Ising circuit is subject to both bit-flip X and phase-flip Z errors, manifesting themselves in the random measurement outcomes of the bond and the site qubits, respectively. Using a gauge transformation as illustrated in Eq. (1), these random Paulis can be propagated to the final times, leaving an Ising circuit where each imaginary-time evolution step is characterized by a position-dependent binary random number, see Fig. 2. The locations of these gates with negative evolution time-steps form a string, whose end points correspond to fixed e and m -vortices [80], see Fig. 2(b). In other words, an e -vortex necessarily pulls a string that changes the sign of β' , while m pulls a string that changes the sign of β . The Ising evolution gates are then coupled to the random bond variables

$$M_Z = \exp\left(\frac{\beta}{2} \sum_j s_{j,y} Z_j Z_{j+1}\right), \quad M_X = \exp\left(\frac{\beta'}{2} \sum_j t_{j,y} X_j\right), \quad (7)$$

where the negative sign $s_{x,y} = -1$ occurs when an m string goes across the bond, and $t_{x,y} = -1$ when an e string goes along the bond, determined by the configuration $|em\rangle$, see Fig. 2(a) [81].

Non-unitary measurement-based quantum computation

We started our discussion of the (1 + 1)D monitored quantum circuit model with an analogy to the framework of measurement-based quantum computation (MBQC) [75, 76]. Let us close this discussion by pointing out some additional connections and distinctions in this context. Similar to the MBQC approach, we initiate our protocol from a cluster state as the principal entanglement resource and perform projective measurements in the bulk to propagate a 1D quantum state on the edge by means of quantum teleportation, trading time with space [82–86]. In the standard MBQC approach, the transfer matrix that evolves the quantum state was shown to be *unitary* and can be universal when the measurement angles are carefully chosen to lie along Z direction or restricted within the XY plane [76]. Then the measurement outcome is maximally random because each post-measurement unitary trajectory shares equal probability, as in the standard example of quantum teleportation with perfect entanglement resource [87]. In the absence of noise one can always correct the

measurement outcomes to obtain the same pure state. In contrast, in our protocol we tilt the measurement angle between Z and the XY plane [4, 88] (equivalent to an imperfectly prepared cluster state [3]), which turns the effective spatial propagation into a probabilistic *non-unitary* [89] circuit. The measurement outcome is no longer maximally mixed but follows a highly correlated distribution. Not all post-measurement random pure states are guaranteed to be able to be corrected to the same pure state.

B. 2D Classical statistical model

The probability distribution function of the boundary 1D states $|\psi(em)\rangle$, conditioned upon a given bulk classical configuration $|em\rangle$ in Eq. (2), follows from Born's rule

$$P(em) = \langle \psi(em) | \psi(em) \rangle \propto \mathcal{Z}(em)^2, \quad (8)$$

where we map the norm of the (1 + 1)D quantum state to the partition function of a doubled 2D classical statistical model

$$\mathcal{Z}(em) = \sum_{\sigma} e^{\frac{\beta}{2} \sum_{ij} s_{ij} \sigma_i \sigma_j} \prod_{ij} (\sigma_i \sigma_j)^{\frac{1-t_{ij}}{2}}. \quad (9)$$

It expresses an Ising model with random bond disorder in both the original lattice and its dual lattice (or imaginary coupling strength), indicated by the dashed line in Fig. 2(b). Here i, j denote the sites, and $\sigma = \pm 1$ corresponds to the 0 and 1 of the site qubit, which has been projected to the $|\pm\rangle = (|0\rangle \pm |1\rangle) / \sqrt{2}$ state with a measurement-outcome-dependent sign factor. The sign factor is given by the e -vortex at the site, which is the end point of the string with $t_{ij} = -1$. On the other hand, $s_{ij} = \pm 1$ is the random measurement outcome on the bond, and a string of $s_{ij} = -1$ in a dual lattice terminates at the m -vortex. The square $|\cdot|^2$ is because of the norm that contracts the ket and bra layers, or the forward and backward propagation of space-time, which also guarantees the positiveness of the probability. Upon a KW duality transformation for the 2D model that exchanges vertex and plaquette, one can verify that $s_{ij} \leftrightarrow t_{ij}$, and $\beta \leftrightarrow \beta'$ [90]. Upon a vertex plaquette duality [40], this random Ising model remains invariant.

If we now trace out half of the vortices, we are left with a random-bond Ising model (RBIM) in both cases

$$\begin{aligned} P(m) &= \sum_e P(em) \propto \sum_{\sigma} e^{\beta \sum_{ij} s_{ij} \sigma_i \sigma_j}, \\ P(e) &= \sum_m P(em) \propto \sum_{\mu} e^{\beta' \sum_{pq} t_{pq} \mu_p \mu_q}, \end{aligned} \quad (10)$$

which are the standard RBIM with gauge symmetrized random bond disorder [2, 3]. Here μ_p is the dual Ising spin residing at the plaquette center, and with $t_{pq} = t_{ij}$ (where ij and pq share the same link) this turns into a random-bond Ising model on the dual lattice. One can derive the density of vortices by:

$$\begin{aligned} 1 - 2\langle m \rangle &= \langle \prod_{\langle ij \rangle \in \square} s_{ij} \rangle = \tanh^4 \beta = \sin^4 \theta, \\ 1 - 2\langle e \rangle &= \tanh^4 \beta' = \cos^4 \theta. \end{aligned} \quad (11)$$

Namely, at the self-dual point ($\theta = \pi/4$) we expect the two vortex densities to cross, i.e. $\langle e \rangle = \langle m \rangle$, which is precisely what we find also in our numerical sampling as shown in Fig. 3(a) below.

Free energy and central charge

All the classical statistical models that capture the transitions discussed in this paper exhibit transitions described by conformal field theories (CFTs) with central charge $c = 0$ [91–93]. To explain this vanishing central charge, it is important to define precisely how a notation for the free energy can be defined for such models. For the Born probability measure $P(em)$, one natural way to do so is to define a family of replicated partition functions by summing over trajectories (measurement outcomes) and their corresponding free energy

$$\begin{aligned} \mathcal{Z}_N &= \sum_{em} P(em)^N, \\ F_N &= -\ln \mathcal{Z}_N. \end{aligned} \quad (12)$$

Physical quantities are obtained in the replica limit $N \rightarrow 1$, corresponding to a Born weighting of the trajectories associated with the trivial partition function

$$\mathcal{Z}_{N=1} = \sum_{em} P(em) = 1. \quad (13)$$

Different replica numbers N have transitions described (for replica number small enough) by CFTs with central charge $c(N)$, with $c(N \rightarrow 1) = 0$ since the free energy in the replica limit $F_{N=1} = 0$ has trivial finite-size scaling. This central charge $c = 0$ is a general feature of all mixed state (measurement-induced) phase transitions studied in this paper, even the so-called Ising+ transition we will encounter below where for some observables, averages like $\sum_{em} P(em) O_{em}$ reduce to Ising correlators (a CFT with central charge $c = 1/2$).

In analogy with classical disordered systems described by logarithmic-CFTs [91–97] with central charge $c = 0$, a more useful quantity is the *effective central charge*

$$c_{\text{Casimir}} = \lim_{N \rightarrow 1} \frac{dc(N)}{dN}, \quad (14)$$

which governs the finite-size scaling of the quenched average free energy

$$\begin{aligned} F &= \lim_{N \rightarrow 1} \frac{dF_N}{dN} = - \sum_{em} P(em) \ln P(em) \\ &= \text{const} \cdot L_x L_y - c_{\text{Casimir}} \cdot \frac{\pi}{6} \frac{L_y}{L_x} + \dots, \end{aligned} \quad (15)$$

when being placed on a length- L_y long cylinder of finite width $L_x \ll L_y$ [98] (see the inset of Fig. 4(a) for a schematic). This formula follows from the general scaling form of the free energy F_N at criticality expected from conformal invariance [98]. The universal number c_{Casimir} captures how the vacuum energy responds to the finite scale of the system,

which is analogous to Casimir effect where the finite width system can save some energy. In this context, the free energy F then acquires physical meaning as the Shannon entropy of the bulk of the mixed 2D state Eq. (2), also called the entropy of the measurement record of the 1+1D monitored dynamics [92], or the frustration entropy of the random classical statistical model [2].

C. (1+1)D monitored Majorana circuit

The random Ising circuit introduced in the previous Section can be mapped to a Majorana quantum circuit [99] via a Jordan-Wigner transformation, see Fig. 2(c). In detail, the L_x qubits can be Jordan-Wigner transformed to $2L_x$ Majoranas γ_j , according to $X_j = i\gamma_{2j-1}\gamma_{2j}$ and $Z_j = \prod_{k=1}^{j-1} (i\gamma_{2k-1}\gamma_{2k})\gamma_{2j-1}$. The non-unitary gates are transformed to the Gaussian evolution generated by the Majorana bilinears $Z_j Z_{j+1} = i\gamma_{2j}\gamma_{2j+1}$ and $X_j = i\gamma_{2j-1}\gamma_{2j}$. Then the GHZ state at $\theta = \pi/2$ in the spin representation is mapped to the topologically nontrivial Majorana state with Majorana zero modes γ_1 and γ_{2L_x} on the edges [49]. The problem is then mapped to a measurement-only Majorana fermion chain weakly monitored by local fermion parity measurements of the nearest-neighbor Majorana fermion bilinears above [100]. The global Ising symmetry is mapped to the total fermion parity $\prod_j X_j \propto \prod_j i\gamma_{2j-1}\gamma_{2j}$, and the KW dual transformation is mapped to a single-site Majorana fermion translation

$$\text{KW: } \gamma_j \rightarrow \gamma_{j+1},$$

see the box in Fig. 2(c). The corresponding self-dual critical point is a monitored Majorana chain with statistical (“averaged”, or “weak”) translational invariance which separates trivial and topological phases upon dimerization [49] of the measurements, and is described by the $N \rightarrow 1$ limit of the 2D Non-linear Sigma Model (NLSM) in symmetry class D with target space $SO(2N)/U(N)$ and topological angle- $\theta = \pi$ [11, 101]. This critical point was studied numerically in the context of a continuously weakly-monitored [102] Majorana chain in Ref. 103. (As expected on general grounds, the continuously weakly-monitored chain falls into the same universality class as our spacetime isotropic model, see Appendix C.)

The replica limit $N \rightarrow 1$ arises [104, 105] because of the Born probability weighting: the case of generic uncorrelated quenched disorder, corresponding to a replica limit $N \rightarrow 0$, is dramatically different and moreover exhibits a Majorana metallic phase [106, 107] which is absent in the $N \rightarrow 1$ limit – see the following Section.

D. (2+1)D Chalker-Coddington network model

Making contact with the body of previous work on Anderson localization [11, 106, 107], the (1+1)D Majorana circuit can be described [108], for any fixed configuration of e and m “vortices”, equally as the ground state of a system of non-interacting Majorana fermions in two spatial dimensions, i.e.

in (2+1)D spacetime dimensions at zero energy (chemical potential). For the system under consideration this is a superconductor in two spatial dimensions in Altland-Zirnbauer [109] symmetry class D. As discussed in [108], the two-dimensional space (Fig. 2(d)) of the (2 + 1)D system represents the spacetime of the circuit depicted in Fig. 2(a,c), and in a formulation of the (2+1)D system on a 2D spatial lattice and discrete time, this is referred to as a “Chalker-Coddington” model [110]: In each time-step of the discrete time the Majorana fermions propagate across a link of a square lattice [the so-called “surrounding lattice” [111], whose sites are the midpoints of the links of the lattice in Fig. 2(d)] whose plaquette-centers represent the locations of Ising spins (σ_i) on one sublattice, and dual Ising spins (μ_p) on the other sublattice of the bipartite lattice of plaquettes, see Fig. 2(c). A spin (σ_i) and dual spin (μ_p) located at (the center of) a plaquette corresponds to a (2 + 1)D vortex enforcing a minus sign for fermions encircling the plaquette in the time of the (2 + 1)D system. In this formulation, a negative sign of the variable “ s_{ij} ” appearing in the transfer matrix, Eq. (7), corresponds to a pair σ_i, σ_j of vortices on nearest-neighbor sites i and j of the sublattice of *spin* plaquettes, while a negative sign of the variable “ $t_{p,q}$ ” in Eq. (7) corresponds to a pair μ_p, μ_q of vortices on nearest-neighbor sites p and q of the sublattice of *dual-spin* plaquettes. In this language, the square of the partition function of the Ising model in any fixed configuration of e and m vortices (in a particular gauge) is obtained (see [106]) by tracing over (two identical copies of Majorana, or equivalently a single copy of complex) fermions, which we denote by $\mathcal{Z}(e, m)$. (See Eq. (9) below, where the same trace is computed, equivalently, in the Ising spin formulation.)

As mentioned, the so-described formulation using the Chalker-Coddington model is given in a *fixed* configuration of the vortices mentioned above, or equivalently (by a gauge choice) of e and m vortices. Historically, such a Chalker-Coddington model was (a) applied to various settings of generic (“uncorrelated”) *quenched* disorder averages over configurations of Majorana fermion zero modes (e and m vortices) [11, 106, 107]. In a theoretical description using replicas, these situations correspond to the limit of the number N of replicas going to zero, $N \rightarrow 0$. In the present work we apply, (b), the aforementioned Chalker-Coddington model to settings where e and m vortices are *measured*, and we are thus interested in quenched *measurement* disorder subjected specifically to the Born-rule probability distribution. In a theoretical description using replicas, these situations correspond [104, 105] to the limit of the number N of replicas going to unity, $N \rightarrow 1$. In both applications, (a) and (b), Kramers-Wannier duality – meaning the invariance of the respective *probability distribution* under Kramers-Wannier duality, also called “statistical”, or “weak”, or “average” Kramers-duality – plays an essential role for the resulting physical behavior of the system.

Relationship with previous work

The key conclusion of the prior work in Refs. [11, 106, 107] was that there are two fundamentally different situations, leading to very different physical properties: case (i), discussed below, which does not exhibit a metallic phase, as well as case (ii) discussed below which does exhibit a metallic phase. We discuss those now in turn, with support of the schematics in Figs. 2(e,f):

- (i) In the case of the RBIM, in its entire phase diagram *at and away from the Nishimori line*, the vortices are allowed to appear only on *one* sublattice of plaquettes of the Chalker-Coddington model, namely on the sublattice of (say) *spin* plaquettes. In this case, only two phases are possible [112], a ferromagnetic (topological) phase and a paramagnetic (topologically trivial) phase. In the RBIM these vortices occur in adjacent pairs. Each such pair corresponds to a negative sign of the random variable s_{ij} described in the first paragraph of this section. This model, the RBIM case (i), *maximally* violates statistical (“average”) Kramers-Wannier symmetry since vortices are only allowed to occur on *one* of the two sublattices of plaquettes [113], the (say) sublattice of *spin* plaquettes.
- (ii) If, on the other hand, Majorana zero modes are also allowed to appear on the other sublattice of plaquettes of the Chalker-Coddington model, namely the sublattice of *dual-spin* plaquettes where they occur in adjacent pairs, then in addition to the ferromagnetic (topological) and paramagnetic (topologically trivial) phases, a third, *metallic* phase will occur in the phase diagram. This is the so-called *Cho-Fisher* (CF) model, originally intended [114] as a formulation of the Nishimori system (a), but later shown [11, 106] to actually describe a different system with the novel properties described in [106, 107] and reviewed here. It should also be noted that it was proven in [106] that a metallic phase is forbidden when vortices are only allowed to occur on one sublattice of plaquettes of the Chalker-Coddington model, as is the case in the Nishimori model, case (a). A variant of the CF model was also discussed in [107] where vortices occur randomly with some probability on *any* site of the two sublattices of plaquettes of the Chalker-Coddington model, but with equal probability on *both* sublattices (dubbed the $O(1)$ -model). This system was shown to exhibit *only* the metallic phase throughout its entire phase diagram, and no ferromagnetic nor paramagnetic phases whatsoever survives infinitesimal disorder strength.

We now discuss the two cases of distinct replica limits:

- (a) $N \rightarrow 0$ replica limit, *uncorrelated quenched disorder*.– The phase diagram of the CF model, case (ii), exhibits a line possessing average Kramers-Wannier symmetry along the phase boundary separating ferromagnetic (topological) and

paramagnetic (non-topological) phases, and connecting the *non-random (pure)* Ising critical point with a multicritical point at which a transition to the metallic phase sets in, and continuing into the metallic phase. This self-dual line is depicted as the vertical line in Fig. 2(f) [107]. Recent numerical work [115] found that the RG flow *emerges* from the multicritical point and flows *into* the pure Ising critical point which (obviously) possesses “strong” as opposed to “statistical” (“weak”, or “average” – in recent jargon) KW symmetry.

(b) *$N \rightarrow 1$ replica limit, Born measurement disorder.*– The previous work [11, 106, 107], briefly summarized in item (a) above, raises the question about the nature of these various phases and transitions when the quenched randomness does not originate from generic, uncorrelated randomness, but rather from *measurements* of the e and m degrees of freedom (representing $(2+1)$ D vortices) satisfying the Born-rule probability distribution. This question has, in fact, been the very motivation for the work that we report in the paper at hand and is what we will address in the following.

It is useful to begin with the KW self-dual system which, in the above-reviewed language of the Chalker-Coddington model, is a version of the KW-self-dual line of the CF model, where however now randomness arises from measurements of e and m , and is thus subjected to the Born-rule probability distribution. In short, we will demonstrate that the KW self-dual model is a “measurement-version” of the CF model discussed in (a) (ii) above, in which the generic quenched disorder is replaced by the intrinsic randomness of quantum mechanical measurement outcomes. In that sense, the KW self-dual system is a self-dual ‘cousin’ of the Nishimori critical point (and it will be in a different universality class, as we also numerically confirm - see Table I).

As the self-dual circuit is a circuit of non-interacting fermions in Altland-Zirnbauer symmetry class D, it is generically described [108, 116–118] by a NLSM with target space $SO(2N)/U(N)$ where N is the number of replicas. Moreover, following the same logic used in Ref. [119] for symmetry class DIII, the case of randomness arising from measurements satisfying the Born-rule probability distribution requires [104, 105] taking the replica limit $N \rightarrow 1$. In addition, and importantly in the present context, Ref. [11] established averaged KW duality of this NLSM. As the topology of the target space $SO(2N)/U(N)$ allows for a Θ -term, criticality is known to occur when $\Theta = \pi$. [This is in complete analogy with, e.g., the familiar $O(3)$ -NLSM, describing the 1D Heisenberg chain.] In summary, this establishes the description of the KW self-dual point by the $SO(2N)/U(N)$ NLSM at Θ -angle $\Theta = \pi$ in the limit $N \rightarrow 1$. (We note that independent work in [101] arrived at the same conclusion about the fixed point, starting from the microscopic (‘lattice’) formulation of Majorana fermion parity measurements.) Moreover, Ref. [11] also found that the $SO(2N)/U(N)$ NLSM as $N \rightarrow 1$ is stable under RG to a certain class of deformations (not necessarily related to the ones we study numerically in the present paper). It is worth noting that with Born-rule measurements there is, in contrast to generic, uncorre-

lated quenched randomness [discussed in part (a) above], no stable metallic phase. This is easily understood as a consequence of the known RG beta function of the coupling constant of the NLSM on this symmetry class D target space (reproduced, e.g., in [11]), which demonstrates stability of the metallic phase in the replica limit $N \rightarrow 0$, relevant for case (a), while in the replica limit $N \rightarrow 1$, relevant for case (b), the metallic phase is unstable. The phase diagram that thus emerges for the measurement-version of the CF model with Born-rule measurements is that depicted in Fig. 2 above (the same as Fig. 1 of Ref. [107]), except that the metallic phase is completely removed: There is then a vertical line describing the self-dual model connecting the non-random (pure) critical Ising point (bottom) with the KW self-dual fixed point (top). Moving to the right or to the left of this vertical line breaks statistical KW duality and leads to the ferromagnetic (topological) or paramagnetic (topologically trivial) phase. These are described by moving the Θ -angle of the NLSM away from π in one direction or the other.

IV. THE SELF-DUAL CRITICAL STATE

Let us start our discussion of mixed-state boundary criticality by characterizing the self-dual critical state first. Using numerical simulations, we first confirm its precise location at $\theta = \pi/4$ by calculating the coherent information for tuning the measurement angle θ along the center line ($p_s = p_\eta = 0$) of in our phase diagram in Fig. 1(c). Such scans for different system sizes also allow us to extract the correlation length exponent ν from a finite-size scaling analysis. We then turn to the entanglement properties of the self-dual critical state and calculate a central charge proxy for its non-unitary CFT description by calculating Calabrese-Cardy-like entanglement arcs whose scaling prefactor $c_{\text{ent}}^{\nu N}$ appearing in the coefficient of the logarithm of subsystem size of the von Neumann entanglement entropy we determine.

A. Coherent information

The mixed-state phase transition of a long-range entangled phase upon decoherence can be diagnosed by the coherent information [6, 42, 120–123], utilizing the fact that a long-range entangled phase can serve as a logical memory. In order to determine the coherent information, which indicates whether this logical memory is still intact, one employs a reference qubit R , whose state maximally entangles with the logical qubit state of the memory. For instance, when viewing the GHZ state as a repetition code, one would entangle the reference qubit together with the initial qubit chain to form a joint GHZ state $|\psi_0\rangle_{QR} = |00\dots 00\rangle_Q \otimes |0\rangle_R + |11\dots 11\rangle_Q \otimes |1\rangle_R$, as shown in Fig. 3(b). When viewed from the Majorana fermion representation, this protocol can alternatively be interpreted as encoding and decoding the logical information in a Kitaev Majorana chain-based topological quantum computation setting [124]. In the topologically nontrivial phase of the Majorana chain [49], the unpaired Majoranas at the boundaries

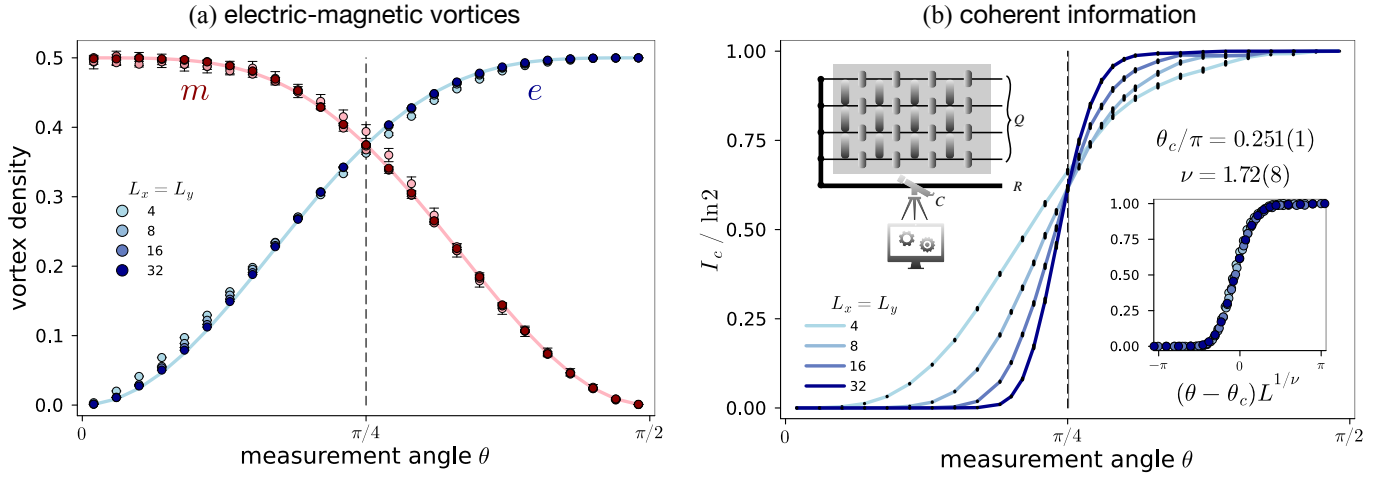


FIG. 3. **Self-dual mixed state transition.** (a) Vortex densities. Shown are numerical (Monte Carlo) results for the e -flux density $\langle e \rangle$ and m -flux density $\langle m \rangle$ as a function of θ for different system sizes L_x . The solid lines are the analytic predictions of Eq. (11). It witnesses the electric-magnetic duality at $\theta = \pi/4$ where the density of the electric charges coincide with the density of the magnetic charges. The vertical line indicates the self-dual location, where the sampled e and m -vortex density becomes identical. (b) Coherent information across the self-dual mixed state transition. The coherent information can be computed as shown in the schematic inset on the upper left: Logical information of R is encoded into the quantum chain (Q), which then undergoes a monitored quantum evolution. An external observer “eavesdrops”, attempting to recover the logical information – with the coherent information reflecting the success of this recovery (with $I_c = \ln 2$ indicating perfect recovery). The solid vertical line indicates the critical point $\theta_c = 0.251(1)\pi$ (fitted via the data collapse shown in the lower right inset), which agrees with the exactly known self-dual location $\pi/4$ within its error bar. In our numerical computation, 100 ~ 1000 independent m configurations are sampled and 1000 Monte Carlo sweeps for e configurations are performed. For $\theta < 0.2\pi$, we initiate from e -vortex-free for Monte Carlo sampling, while for $\theta > 0.2\pi$ we initiate from random vortex configurations.

form, within their topologically degenerate 2-state manifold, a mixed state of even and odd parities. This mixed state corresponds to a 2-dimensional logical code space without any encoding yet. It can, however, be purified by maximally entangling it with a reference qubit R [120].

The logical information being encoded into the system spreads through the bulk evolution, and meanwhile keeps being “eavesdropped” by the local measurements of an observer [125, 126], such that the spacetime evolution can be interpreted as a faulty channel. Whether the quantum logical information is stolen by the observer or whether it is still preserved in the system, is what is quantified by the quantum coherent information [6, 121–123]

$$I_c = S_{\text{vN}}(\rho_{QC}) - S_{\text{vN}}(\rho_{QCR}), \quad (16)$$

where we have included an additional index C indicating the existence of classical information (obtained from measurements) accessible for a decoder. In our setup, C refers to the bulk bits that are fully dephased after the measurement and $\rho_{QC} = \bigoplus_{em} P(em)\rho_Q(em)$ is a block-diagonal matrix where each block corresponds to a different measurement outcome. Thus the von Neumann entropies of the 2D mixed state are stemming from two parts – the Shannon entropy of the bulk classical bits, and the trajectory-averaged von Neumann entropy of the boundary quantum bits [127]

$$\begin{aligned} S_{\text{vN}}(\rho_{QC}) &= -\text{tr}(\rho_{QC} \ln \rho_{QC}) \\ &= F + \sum_{em} P(em) S_{\text{vN}}(\rho_Q(em)). \end{aligned}$$

Consequently, the coherent information (16) reduces to the trajectory-averaged conditional entropy

$$I_c = \sum_{em} P(em) (S_{\text{vN}}(\rho_Q(em)) - S_{\text{vN}}(\rho_{QR}(em))). \quad (17)$$

Under the measurement channel, each trajectory em yields a pure post-measurement state. Then $S_{\text{vN}}(\rho_{QR}(em)) = 0$ and $S_{\text{vN}}(\rho_Q(em)) = S_{\text{vN}}(\rho_R(em))$. As a result, Eq. (17) reduces to a measurement average of the entanglement entropy between the system and the reference qubit [121]

$$I_c = \sum_{em} P(em) S_{\text{vN}}(\rho_R(em)).$$

Cast in the language of the random Ising statistical model, the reference qubit R determines the boundary condition of the Ising layers. The density matrix element of R is determined by the partition function under the corresponding boundary conditions, which can be represented by the tensor network as follows:

$$\begin{aligned} \langle 0 | \rho_R | 0 \rangle &= \\ \langle 0 | \rho_R | 1 \rangle &= \end{aligned}$$

for a given typical snapshot of em . Here for $\langle 0|\rho_R|0\rangle$ the boundaries of both layers are pinned to product state 0; in contrast, for $\langle 0|\rho_R|1\rangle$ the boundaries of the two layers are pinned to the opposite directions, which means a non-contractible domain wall or twist-defect line is inserted to the bulk, indicated by the shaded red string in the diagrammatic equation. The global Ising symmetry of the network guarantees that $\langle 0|\rho_R|0\rangle = \langle 1|\rho_R|1\rangle$ and $\langle 0|\rho_R|1\rangle = \langle 1|\rho_R|0\rangle$. The resultant coherent information, equal to the entropy of R , is determined by the *absolute* ratio $|\langle 0|\rho_R|1\rangle|/|\langle 0|\rho_R|0\rangle|$, which is simply the expectation value of inserting a domain wall defect. In the ordered phase $\theta \rightarrow \pi/2$, the domain wall decays exponentially with system size, $\langle 0|\rho_R|1\rangle/\langle 0|\rho_R|0\rangle \propto \mathcal{O}(e^{-L_x})$, which means that R is almost diagonal and maximally mixed, thereby giving rise to a maximal coherent information $I_c \rightarrow \ln 2$. In the disordered phase $\theta \rightarrow 0$, $\langle 0|\rho_R|1\rangle/\langle 0|\rho_R|0\rangle \propto \mathcal{O}(1)$, and ρ_R converges to a purified state with $I_c \rightarrow 0$. For the non-perturbative regime between these two limits, we perform a hybrid Monte Carlo and Gaussian fermion numerical computation of the coherent information I_c while sweeping θ , which is found to exhibit a clear level crossing near the self-dual point $\theta_c = \pi/4$ as shown in Fig. 3(b). The clean finite-size collapse indicates the critical length exponent $\nu = 1.72(8)$.

At $\theta > \pi/4$ the mixed 1D quantum state is a Z_2 SW-SSB phase. The strong Ising symmetry $(\prod_{j \in Q} X_j)\rho = \rho$ is spontaneously broken as evidenced by the exponential cost of the domain wall, or the long-range fidelity correlator [9]:

$$\text{tr}\sqrt{\sqrt{\rho}Z_iZ_j\rho Z_iZ_j\sqrt{\rho}} = \sum_{em} P(em)|\langle Z_iZ_j \rangle_{em}| \neq 0,$$

where the overlap between the charge-neutral mixed state and its charged counterpart is reduced to the disorder average of the *absolute* value of the spin-spin correlation function, akin to an Edwards-Anderson correlation studied for the same model in Ref. [3]. The resultant state still preserves the *weak* Z_2 symmetry because of vanishing long-range correlation $\text{tr}(\rho Z_i Z_j) = \sum_{em} P(em)\langle Z_i Z_j \rangle_{em} = 0$. Therefore the weak self-dual critical state ($\theta = \pi/4$) separates the SW-SSB ordered phase ($\theta > \pi/4$) from the symmetric trivial phase ($\theta < \pi/4$).

B. Bulk Shannon entropy

Having precisely located the self-dual critical point at $\theta = \pi/4$ also in our numerical simulation, we compute the bulk Shannon entropy at this point and find that it indeed follows the scaling law (15) of a CFT, as shown in Fig. 4(a). Fitting our numerical data we extract an estimate of the effective central charge

$$c_{\text{Casimir}} = 0.437(7),$$

for the self-dual point.

On a more technical note, we calculate this effective central charge estimate for the “vacuum state”, i.e. a state in the even sector for which we enforce the absence of an m -vortex through the hole of the cylinder by restricting $\prod_x s_{x,y=1} = +1$

as a Wilson loop surrounding the cylinder along the first column, which is akin to the periodic boundary condition of the clean Ising model without disorder. For this vacuum state, the typical scaling dimension of the m -vortex determines the typical correlation between two far separated m -vortices [12]. It can be deduced from the energy cost of threading an m -vortex through the hole of the long cylinder, which pulls a semi-infinite long line defect through the cylinder, see the inset of Fig. 4(a) for a schematic, equivalent to changing the boundary condition from periodic to antiperiodic. From the perspective of the 2D mixed state, this energy cost is equivalent to the relative entropy between the even and odd sector of the mixed state, when the density matrix is divided into two blocks according to the absence or presence of an m -vortex through the hole of the cylinder:

$$\frac{F_1 - F_0}{L_y} = - \sum_{em} P(em) \ln \frac{P_1(em)}{P(em)} \propto \frac{2\pi\Delta_m}{L_x}, \quad (18)$$

where $P_1(em)$ is the partition function with an extra m -vortex through the cylinder hole, given the same em configuration in the bulk. The additional entropy scales with a universal scaling dimension of the vortex, which from our numerical simulations summarized in the inset of Fig. 4(a), can be extracted to be

$$\Delta_m \approx 0.259(1).$$

Due to the self-duality, the scaling dimension of the e -vortex in the bulk shall be identical to $\Delta_e = \Delta_m$. Note that the e -vortex corresponds to the spin operator σ in Eq. (9), while the m -vortex corresponds to the dual spin operator in the statistical model, which is often labeled by μ [12]. Then the typical spin-spin correlation function in the bulk is governed by the same scaling dimension Δ_e .

Lyapunov spectrum

Besides the vacuum energy alone, one can look into the full (single-particle) Lyapunov spectrum which reveals more information of the $(1+1)$ D dynamics. In particular, we compare the clean Ising, Nishimori, and the weak self-dual criticality, see Fig. 5 below. As a consequence of the underlying 10-fold way (Altland-Zirnbauer) symmetry class D, the single-particle spectrum has particle-hole symmetry, being symmetric with respect to the zero energy level. The even and odd sectors are labeled by the black and red colors. The spectrum becomes denser upon increasing the system size L_x , which can be viewed as forming two “bands” in the thermodynamic limit where the gap closes. The vacuum of the CFT is obtained by fixing the even sector and filling the lower band. Pumping an m -vortex through the cylinder hole traps a Majorana mode, drawing two levels from the band into the middle of the “gap”. They lie at exactly zero energy for the clean Ising critical point, resulting in a two-fold degeneracy of the many-body spectrum due to the Majorana zero mode [49]. However, they split in the Nishimori critical

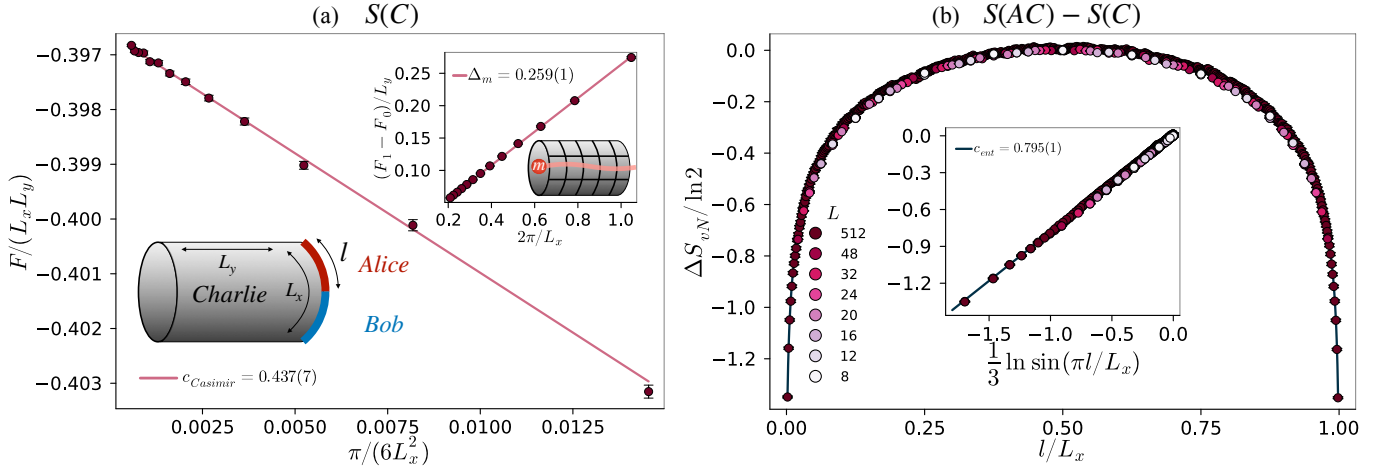


FIG. 4. **Characterization of the self-dual critical theory** via the effective central charge and entanglement scaling at the point $\theta_c = \pi/4$. For the system placed on a cylinder, we label the decohered bulk as “Charlie” (C) and the two segments of the bipartition of the boundary quantum chain as “Alice” (A) and “Bob” (B). (a) The Shannon entropy density of Charlie is equal to the free energy density of the classical statistical model (9), which is governed by the *effective* central charge $c_{\text{Casimir}} = 0.437(7)$. Inset: twisting the boundary condition yields the scaling dimension of the vortex operator being $\Delta_m = 0.259(1)$. The numerical sampling is performed for long cylinder of sizes $L_x = 6 - 30$ and $L_y = 100L_x$ with $\mathcal{O}(1000)$ Monte Carlo samples, where the energy density is extracted deep in the bulk. (b) The von Neumann entropy of Alice conditioned upon Charlie scales logarithmically with the chord length, from which we extract the prefactor $c_{\text{ent}}^{\text{vN}} = 0.795(1)$ as the scaling dimensions of the boundary twist operator. The numerical calculation was performed for cylinder of sizes up to $L_x = 512$ and $L_y \geq 2L_x$ in periodic spatial boundary condition, with 2,000 Monte Carlo sweeps for $L_x = 512$ and 500,000 sweeps for $L_x = 8 - 32$.

state, which we attribute to the hybridization with the background m -vortices in the bulk. For Nishimori we numerically verify that $\Delta_m \approx 0.341(1)$, which roughly agrees with the scaling dimension $2\pi\Delta_m/L_x \approx 0.691(2)\pi/L_x$ reported in Ref. [12, 128, 129], see Appendix A 3 for more details. For the weak self-dual critical state with not only proliferated m -vortices but also proliferated e -vortices, the midgap modes merge to the opposite band, where the m -vortex costs energy proportional to the finite size “gap”. The numerically computed single particle spectrum exhibits a double degeneracy upon threading the m -vortex, which reason remains to be understood.

C. Boundary entanglement entropy

For the 2D mixed state at hand we have identified in our discussion of the coherent information above that its von Neumann entropies stems from two parts – the Shannon entropy of the bulk classical bits, which we have discussed in the previous Section, and a trajectory-averaged von Neumann entropy of the boundary quantum bits. The latter is what we will turn to now.

The von Neumann entropy of the boundary quantum chain exhibits CFT scaling and a Calabrese-Cardy entanglement arc of the form

$$\begin{aligned}
 S_{AC} - S_C &= \sum_{em} P(em) S_{\text{vN}}(\rho_A(em)) \\
 &= \frac{1}{3} c_{\text{ent}}^{\text{vN}} \cdot \ln \left(\frac{L}{\pi} \sin \frac{\pi l}{L} \right) + \dots, \quad (19)
 \end{aligned}$$

when considering the conditional entanglement entropy $S_{AC} - S_C$ with A denoting a segment (of length l) of the quantum chain, where we abbreviate $S_{\text{vN}}(\rho_{AC})$ by S_{AC} (and similarly for all terms in the following). It is equivalent to the measurement trajectory-averaged von Neumann entropy between Alice and Bob, in the notion of the inset of Fig. 4(a). Fitting the entanglement arcs of Fig. 4(b) we can determine the ‘central charge proxy’ (which is the [typical] critical exponent of the boundary condition changing (bcc) twist operator - see below)

$$c_{\text{ent}}^{\text{vN}} \approx 0.795(1).$$

Technically, we perform a free-fermion evolution for a fixed random trajectory em , and use Born’s rule to sample the ensemble of trajectories. In this numerical context, we can easily generalize from the von Neumann entropy to the family of higher-order Rényi entropies and calculate their respective central charge proxy for the Born-averaged ensemble of trajectories (as above). We find that this central charge proxy monotonically decreases towards

$$c_{\text{ent}}^{(\infty)} = 0.484(1),$$

in the ∞ -Rényi-order limit, see Appendix B for supporting numerical data.

While c_{ent} is identical with the central charge for unitary CFTs [98], for the non-unitary CFT situation at hand it captures the (typical) scaling dimension of so-called boundary condition changing (bcc) operators. The latter describe the scaling of bipartite entanglement of the non-unitary boundary CFT [92, 93, 104, 130], and should not be confused

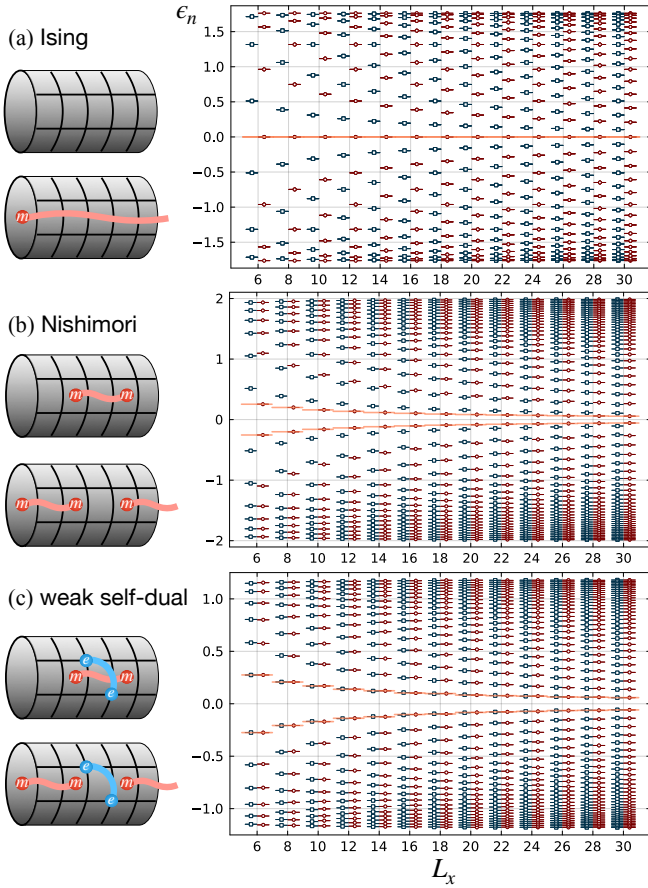
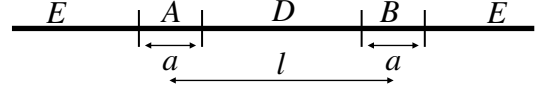


FIG. 5. **Energy or Lyapunov spectra.** Shown are the free-fermion energy or Lyapunov spectra for a cylinder of finite width for the Ising, Nishimori and weak self-dual critical states, respectively. For each case, we show schematically a typical vortex configuration in a cylinder in the even sector, compared with its counterpart in the odd sector with an m -vortex threaded into the big hole of the cylinder. The spectrum for the even sector is denoted by the black levels with squared marker, while that for the odd sector is denoted by the red levels with circle markers. The orange lines in the middle of the spectrum highlight the “midgap” levels as created by the m -vortex threaded to the cylinder hole. (a) For the clean Ising critical state placed on a cylinder of finite width (a quasi-1D system), an m -vortex pulls two fermion states from the band onto the mid-gap zero-energy level, forming a pair of exact Majorana zero modes, akin to the topological Majorana chain [49]. (b) A hybridization with the background m -vortices results in the energy splitting of the zero modes. (c) In the presence of e -vortices, the midgap modes merge into the opposite bands and the fermionic spectra are degenerate between the two sectors.

with c_{Casimir} , a universal finite-size scaling amplitude at criticality, which can be extracted, as discussed in the previous Section, from the Shannon entropy of the measurement record [92, 93, 130].

The scaling dimension c_{ent} also determines the conditional mutual information (CMI), a non-linear correlation related to the reversibility of the quantum channel, which can signal the mixed state phase transition point [131]. For this quantity we can partition the 1D chain into 4 segments, denoted by

A, B, D, E , respectively, with the length being $|A| = |B| = a$, $|D| = l - a$ such that the distance between the centers of A and B is l :



Then we investigate the CMI scaling with distance as a function of L_x . By making use of the block diagonal property of the density matrix, the Shannon entropy is subtracted from the CMI of the total system, which is reduced into the Born average of the CMI of each post-measurement pure state

$$I(A : B|D) = \sum_{em} P(em) (S_{AD} + S_{BD} - S_D - S_{ABD})_{em}. \quad (20)$$

Each term is the Born-averaged entanglement entropy of a contiguous block, which is a function of its length only, due to its average translation symmetry. We consider the regime $a \ll l$. In the area law phase, S saturates to a constant $\sim \ln \xi$ that depends only on the characteristic length scale but not the subsystem size, and thus $I(A : B|D) \sim 0$, signaling a non-zero Markov gap and finite Markov length. At the critical point, using the numerically confirmed scaling law Eq. (19), we find

$$I(A : B|D)|_{\theta=\pi/4} = \frac{1}{3} c_{\text{ent}}^{\text{vN}} \cdot \ln \frac{\sin^2(\frac{\pi l}{L})}{\sin(\frac{\pi(l-a)}{L}) \sin(\frac{\pi(l+a)}{L})} \sim \begin{cases} \frac{1}{3} c_{\text{ent}}^{\text{vN}} \cdot \frac{a^2}{l^2} & , l \ll L \\ \frac{1}{3} c_{\text{ent}}^{\text{vN}} \cdot \frac{\pi^2 a^2}{L^2} & , l = L/2 \end{cases} \quad (21)$$

which decays in an inverse square law with a universal prefactor $c_{\text{ent}}^{\text{vN}}/3$. Physically, the divergence of the Markov length implies the *irreversibility* of the channel which occurs at the critical point that separates two distinct mixed state phases [35, 131].

V. MIXED-STATE PHASE DIAGRAM AND RG FLOWS

Let us now move away from the self-dual line ($p_s = p_\eta = 0$) in our phase diagram of Fig. 1(c) and consider two perturbations that both explicitly break self-duality. First in the form of incoherent noise (upper half in our phase diagram), then in form of a coherent deformation (lower half in our phase diagram) and, last but not least, we restore the strong self-duality by a duality-preserving coherent deformation.

A. Breaking self-duality by measurement noise

The presence of imbalanced measurement noise explicitly breaks the self-duality. Here we consider measurement noise for the site qubit, controlled by a parameter p_s . For the intermediate topological toric code, the measurement noise of the e -vortices introduces an effectively finite temperature which,

in two spatial dimensions, immediately destroys its topological order [132, 133]. Nonetheless, the boundary phase transition persists even in the presence of this noise and turns into the Nishimori transition for $p_s = 50\%$. In this limit, it is equivalent to tracing out the site qubits and can be mapped to the RBIM in the replica limit $N \rightarrow 1$, thus rigorously corresponding to the Nishimori transition [3–5]. Upon close inspection of the scaling behavior at the boundary phase transition upon introducing the noise, we find that its universality qualitatively changes immediately, indicating an RG flow from self-dual criticality to Nishimori as we will discuss in the following. Similar considerations can, by duality, be applied to m -vortex noise.

In the presence of a measurement error the state corresponding to each of the bulk classical states $|em\rangle$ becomes a noisy mixed state

$$|\rho(em)\rangle\rangle = \sum_{e'} P(e'|e) |\psi(e'm)\rangle\rangle, \quad (22)$$

where e is the measurement record, while e' is the vortex that the Majorana fermion truly experiences, whose correlation is determined by the noise probability: $P(e'|e) = (1 - p_s)\delta_{e',e} + p_s(1 - \delta_{e',e}) = P(e|e')$ for each individual site independently. Here we use the double-ket notation to denote the density matrix as a purified state in the doubled Hilbert space [7, 8, 68–70, 122, 134, 135], which is sometimes referred to as ‘‘Choi state’’, due to the Choi-Jamiolkowski isomorphism [136, 137] that maps a channel to a state. For example, for a pure state $|\psi(em)\rangle\rangle = |\psi(em)\rangle \langle\psi(em)|$ its Choi state is simply a tensor product of the two states, which can be further glued by the noise Kraus operators, see Fig. 6(a) for schematic and Appendix Sec. A 4 for tensor network diagrammatic representation. The trace of the original physical qubits is equivalent to an overlap with a Bell state between the ket and bra: $\text{tr}\rho = \langle\langle\text{Bell}|\rho\rangle\rangle$, while the purity becomes the norm of the Choi state: $\text{tr}\rho^2 = \langle\langle\rho|\rho\rangle\rangle$. Thus the corresponding Born’s probability is also accordingly distorted by the noise: $\tilde{P}(em) = \langle\langle\text{Bell}|\rho(em)\rangle\rangle = \sum_{e'} P(e'|e)P(e'm)$.

The noisy mixed state is no longer Gaussian in the Majorana representation, whose von Neumann coherent information is therefore hard to compute generically. However, we can turn to a Born measurement average of the second Rényi coherent information by adapting Eq. (17), as it is a *linear* physical observables w.r.t. the Choi state

$$\begin{aligned} I_c^{(2)} &= \sum_{e,m} \tilde{P}(em) [S_Q^{(2)}(em) - S_{QR}^{(2)}(em)] \\ &= \sum_{e,m} \tilde{P}(em) [-\ln\langle\langle\hat{B}_R\rangle\rangle], \end{aligned} \quad (23)$$

where $\hat{B}_R = 2|\text{Bell}\rangle\rangle_R\langle\langle\text{Bell}|$ is two times of the Bell projector of the reference qubit. Its expectation value can be efficiently calculated by our tensor network representation [138], see Appendix Sec. A 4 for details.

For a generic mixed quantum state, the phase transition and its criticality could depend on the order of the Rényi quantity, as different copies of the density matrices are involved and are mapped to statistical models with different layers [122]. However, in our case here, the limit $p_s = 0$ is an

em -trajectory-resolved pure state whose different Rényi entropies are related to scaling operators within the same critical theory [130]. In the maximal noisy limit $p_s = 50\%$, on the other hand, it becomes an m -trajectory-resolved, fully dephased, diagonal density matrix, whose Rényi entropies all diverge at the same transition point. Specifically, our $p_s = 50\%$ point can be mapped to the 2D RBIM along its Nishimori line [3–5]. Indeed, the numerical exponents we compute in Fig. 6 are consistent with those for the Nishimori criticality in Refs. [42, 128, 129, 139–141]. As shown in Fig. 1(c), for $p_s > 0$ and $\theta > \theta_c$, we expect the boundary state to be dephased in the thermodynamic limit into a classical glassy Ising-ordered mixed state. This is evidenced by the numerically computed noisy coherent information $I_c \rightarrow 0$ under finite-size scaling (see Fig. 11 in Appendix E). The onset of measurement noise leads to a dephasing effect that immediately collapses the logical qubit into a logical classical bit in thermodynamic limit. In the Majorana representation, it means the topological protected logical qubit composed of the two edge Majoranas is unstable against the (noise-induced) proliferation of e -vortices in spacetime. It does not contradict the topological protection because the e -vortices are highly *non-local* topological defects. If a bond measurement error is turned on in addition, the ordered phase and the Nishimori criticality survive until a finite threshold, as realized in a noisy digital quantum processor [5].

RG flow

To understand the renormalization group (RG) flow for the manifold of critical points for $0 \leq p_s \leq 50\%$, we have calculated the entanglement entropy for the Choi state $|\rho(em)\rangle\rangle$. The entropy is averaged over the Born ensemble given by $\tilde{P}(em)$, and agrees with the logarithmic scaling as in Eq. (19) with a scaling prefactor denoted by $\tilde{c}_{\text{ent}}^{(n)}$, which should be distinguished from the pure state ones, $c_{\text{ent}}^{(n)}$. Only in the noiseless limit, where the Choi state is simply a tensor product of the ket and bra wave functions, are the two trivially related by $\tilde{c}_{\text{ent}}^{(n)} = 2c_{\text{ent}}^{(n)}$ due to the additivity property of the entanglement entropies. Estimates in the presence of noise $0 \leq p_s \leq 50\%$ are shown in Fig. 6(a) for the von Neumann entropy prefactor $\tilde{c}_{\text{ent}}^{\text{vN}}$. In addition, we plot the scaling exponents for the Rényi entanglement entropy of the Choi state in Fig. 6(b).

Looking at the data in Fig. 6(b,c), we see a sudden drop of the von Neumann entropy prefactor $\tilde{c}_{\text{ent}}^{\text{vN}}$ upon introducing a finite noise $p_s > 0$, as well as an immediate (though less dramatic) change of the critical exponent ν . What these changes signal, is that the universality of the critical behavior instantaneously changes in the presence of noise – indicating an RG flow towards a different universality class. Specifically, our results imply a decoherence-driven renormalization group flow from the self-dual criticality to Nishimori criticality.

The instability of the self-dual critical point in the presence of noise can be rationalized due to the effect of noise-induced decoherence, which induces unavoidable interactions between the two layers of Majoranas. This raises the question whether

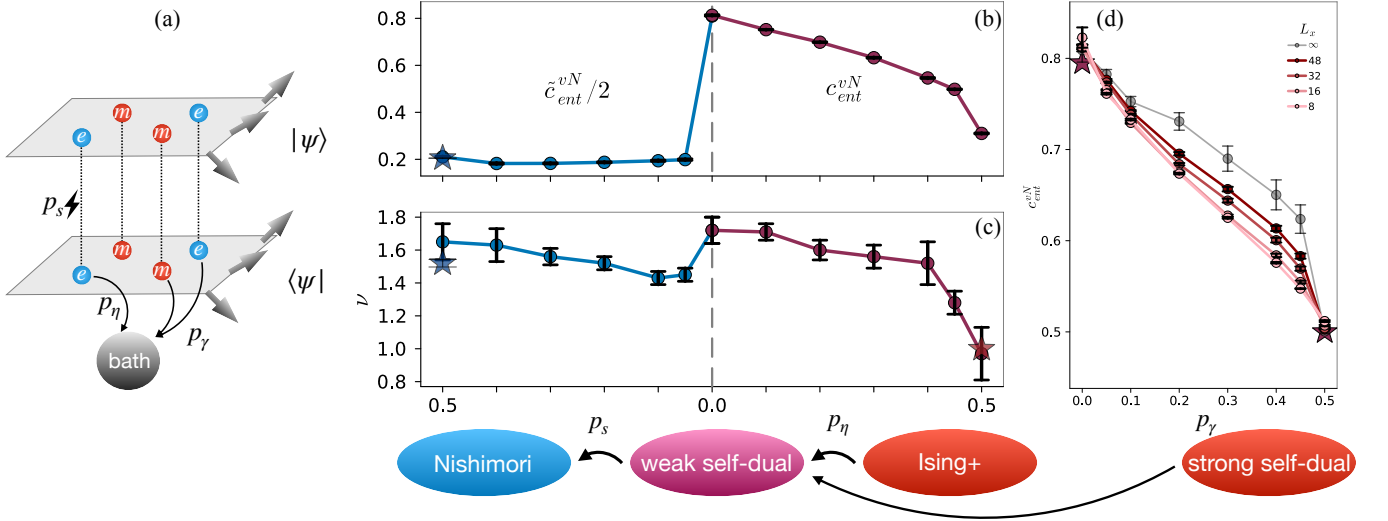


FIG. 6. **RG flow between the critical states**, tracking the critical line in the phase diagram in Fig. 1(c). (a) Schematic of the three types of disturbances. Each layer denotes one tensor network as the spacetime evolution of the $(1+1)$ D quantum state, subjected to random e - and m -vortices. The site measurement noise p_s blurs the e -vortex configuration, the deformation p_η absorbs the e -vortices to the bath, while the coherent deformation p_γ absorbs the e - and m -vortices together, maintaining the self-duality. (b) \tilde{c}_{ent}^{vN} is the scaling exponents for the von Neumann entanglement entropy of the $(1+1)$ D noisy quantum state, viewed as a Choi pure state, where the disorder is averaged according to the Born's rule. c_{ent}^{vN} governs the trajectory averaged pure state entanglement entropy under the coherent deformation. (c) ν is the critical length exponent extracted from FSS for coherent information. At $p_s = 50\%$ the Nishimori critical point, $\nu = 1.65(11)$, $\tilde{c}_{ent}^{vN} = 0.421(5)$ based on our calculation of sizes up to $L_x = 32$. For comparison, the star markers denote the data using larger system size $O(10^3)$ calculation, adapted from Puetz *et al.* [42]: $\nu = 1.52(2)$, $\tilde{c}_{ent}^{vN} = 0.410(1)$. At $p_\eta = 0.5$ the Ising+ critical point, $\nu = 1.00(5)$, $c_{ent}^{vN} = 0.310(2)$. The data is computed by finite size scaling of size $L_x = 4, 8, 16, 32$, whose data collapse is shown in Appendix Sec. E. Here we plot \tilde{c} by half because it expresses the entropy of the Choi state in the double Hilbert space. (d) Flow from strong to weak self-dual symmetry, witnessed by the entanglement entropy scaling exponent c_{ent}^{vN} . Computation is performed in open boundary condition for p_s noisy regime, and periodic boundary condition for p_η and p_γ coherent deformation regime.

there is a way to break the self-duality while preserving the *purity* of the trajectory-resolved Majoranas, which we will now address by considering a *coherent* deformation instead of incoherent noise.

B. Breaking self-duality by deformation

To break self-duality without breaking purity of each trajectory, one can introduce a bath to absorb the e -vortices, or to damp the Pauli X operator of the site qubits. To be concrete, we deform the quantum state by applying a finite-depth local *non-unitary* circuit $\exp(-\eta \sum_j (1 - X_j)/2)$ onto the site qubits, before their measurement. This non-unitary gate has previously been denoted as a “wave function deformation” [45–47, 61]. If not directly implemented in a circuit this deformation can, in principle, also be realized as the ground state of a 2D Rokhsar-Kivelson type Hamiltonian [142]. Consequently, the statistical model (8) picks up an additional weight factor

$$P(em)' \propto \mathcal{Z}(em)^2 \times \exp\left(\frac{\eta}{2} \sum_{\langle ij \rangle \in +} \prod_{\epsilon} t_{ij}\right), \quad (24)$$

up to an em independent normalization constant such that $\sum_{em} P(em)' = 1$. Note that this extra term is reminiscent of a gauge coupling, with η endowing a mass to the

e -vortex. By tuning η from 0 to ∞ , we can thereby control the density of the e -vortices, which completely vanish at $\eta \rightarrow \infty$. This expression can alternatively be viewed as a “reweighting” of the post-measurement Born ensemble. The corresponding $(1+1)$ D circuit is composed by a deterministic $\exp(\beta^t X/2)$ and a monitored (non-deterministic) $\exp(\pm\beta Z_j Z_{j+1}/2)$ imaginary-time evolution. However, caution that the probability of the random gate $\exp(\pm\beta Z_j Z_{j+1}/2)$ at a given time is not only conditioned upon the “past” but also the “future” of the $(1+1)$ D evolution, which is computed by tracing out the whole $(1+1)$ D spacetime sheet.

For convenience we compactify the phase diagram within $p_\eta \in [0, 0.5]$ where $\eta = \ln \frac{1+2p_\eta}{1-2p_\eta}$. In the limit $\eta \rightarrow \infty$, the e -vortices vanish, $P(em)' \propto P(m)'\delta_{e,0}$. In the absence of e , the m -dependent partition function $P(m)'$ reduces to two random bond Ising layers that share the same m -vortex disorder:

$$\begin{aligned} P(m)' &\propto \mathcal{Z}(m)^2 = \sum_{\sigma, \tau} \exp\left(\frac{\beta}{2} \sum_{\langle ij \rangle} s_{ij}(\sigma_i \sigma_j + \tau_i \tau_j)\right) \\ &= \sum_{\sigma, \tau} \prod_{\langle ij \rangle} [1 + \tan^2\left(\frac{\theta}{2}\right) \sigma_i \sigma_j \tau_i \tau_j + s_{ij} \tan\left(\frac{\theta}{2}\right) (\sigma_i \sigma_j + \tau_i \tau_j)], \end{aligned} \quad (25)$$

where we use the fact that $\tanh(\beta/2) = \tan(\theta/2)$, and in the second line we perform a high-temperature expansion.

When the disorder is traced out, the s terms drop out, so we find the normalization constant of the Born probability to be $\sum_m P(m)' \propto \sum_{\sigma\tau} \exp[\tanh^{-1} \tan^2(\theta) \sum_{\langle ij \rangle} \sigma_i \sigma_j \tau_i \tau_j]$, which is a non-random Ising model describing the disorder average correlations of the joint Ising spin $\sigma'_j \equiv \sigma_j \tau_j$. A transition point can then be readily determined via Kramers-Wannier duality

$$\tan^2\left(\frac{\theta_c}{2}\right) = \frac{1}{1 + \sqrt{2}},$$

which yields $\theta_c/\pi = 0.364\dots$

Notably, at this critical point all *disorder-independent* operators are described by the *unitary* Ising CFT, which obeys this self-duality. For instance, the two-point correlation $\langle \sigma'_i \sigma'_j \rangle \sim |i-j|^{-1/4}$ because σ' picks up the scaling dimension $1/8$ from the Ising CFT. Nevertheless, measurement-induced quenched randomness (which also breaks self-duality) causes (random) quantum trajectory resolved quantities to be no longer described by simple unitary Ising CFT, which is the reason why we have dubbed this critical theory “Ising+” theory. As shown in Fig. 6(b), the critical length exponent $\nu = 1.00(5)$ extracted from coherent information agrees with that of the simple Ising CFT. If one looks into the entanglement entropy scaling of the (1+1)D quantum state formed by the joint spins, σ'_j , or its ground state energy scaling, one would recover the central charge $1/2$. In contrast, the measurement-averaged entanglement entropy for our quantum state is expressed for τ spins alone, which yields

$$c_{\text{ent}}^{\text{vN}}|_{\eta=\infty} = 0.310(2),$$

which is a universal number that is not captured by the unitary Ising CFT. Besides, the normalization condition $\sum_m P(m)' = 1$ ensures that this critical point has vanishing central charge following Eq. (12).

Properties characteristic of quenched disorder (including the intrinsic randomness of quantum mechanical measurements, governed by the Born-rule distribution) are described by derivatives with respect to replicas, analogous to the effective central charge – just for different observables. (See, e.g., Ref. 104.) For instance, when formulated within the replica formalism, $c_{\text{ent}}^{\text{vN}}|_{\eta=\infty} = 0.310(2)$ above should be a derivative with respect to N as $N \rightarrow 1$ of the corresponding replicated boundary condition changing (“twist”) operator correlation function computed with N replicas; this is needed to generate an average of a *logarithm* in the entropy. The result $c_{\text{ent}}^{\text{vN}} = 0.310(2)$ comes from the extra $(N-1)$ replicas and the derivative.

As shown in Fig. 6(b)(c), when deviating from the $\eta = \infty$ limit, ν and c_{ent} quickly cross over to the exponents for the self-dual criticality. This again indicates an RG flow, now from Ising+ criticality to self-dual criticality. (Numerical data for the finite-size collapse is shown in Fig. 10 in Appendix E.)

C. Strong to weak self-dual symmetry

If we further add a mass term to not only the e but also the m -vortices, we can maintain the self-dual symmetry while

damping both e and m on equal footing. Such a scenario is captured by a statistical model given by

$$P(em)'' \propto \mathcal{Z}(em)^2 \times \exp\left[\frac{\gamma}{2} \left(\sum_{+ \langle ij \rangle \in +} t_{ij} + \sum_{\square \langle ij \rangle \in \square} s_{ij} \right)\right], \quad (26)$$

where $\gamma = \ln \frac{1+2p_\gamma}{1-2p_\gamma}$. In the limit $p_\gamma = 1/2$, $\gamma = \infty$, all e and m are suppressed and our mixed-state self-dual criticality reduces to the non-random Ising criticality, whose $(1+1)$ D quantum state exhibits self-duality as a strong symmetry

$$\text{KW } |\psi\rangle|_{\gamma=\infty} = |\psi\rangle|_{\gamma=\infty},$$

up to boundary condition terms [143]. This can be visualized in the Majorana representation where the state inherits the Majorana translation symmetry from the Majorana quantum circuit. For any finite p_γ , the self-duality is respected and the point at $\theta = \pi/4$ remains always critical, distinct from the deformation critical line in Fig. 1(c). Therefore we sit at $\theta = \pi/4$ and perform our Born sampling computation for the Born-averaged entanglement entropy to obtain the scaling exponents $c_{\text{ent}}^{\text{vN}}$ as a function of p_γ . As shown in Fig. 6(d), the finite-size fit $c_{\text{ent}}^{\text{vN}}$ for the critical point closer to the clean Ising significantly drift upwards, while that closer to the mixed critical point converges faster. This indicates a crossover from the unitary Ising CFT, with strong self-dual symmetry, to the mixed state self-dual criticality, with only weak self-dual symmetry. For the measurement-version of the Cho-Fisher model at hand the RG flow is thus towards *decreasing* mass, i.e. flowing from pure Ising to the KW-self dual point. Note that this is the *opposite* direction of the RG flow within the conventional Cho-Fisher model in the $N \rightarrow 0$ replica limit [115], which is schematically shown in Fig. 2(f).

VI. DISCUSSION AND OUTLOOK

Summary of RG flows

Stepping back, one result of our study is a cascade of RG flows between different critical theories, see Fig. 6. Putting together all the numerical evidence, one arrives at a flow within the mixed-state critical line from Ising+, to self-dual criticality, and finally towards Nishimori criticality. In other words, when noise sets in, every fixed point could flow to Nishimori criticality – elevating it to a remarkably stable universality class in this context. This adds to the mounting evidence that Nishimori criticality might be an ubiquitous phenomenon in the quantum dynamics of monitored cluster states – it naturally arises from Born’s rule [3], it emerges both in the presence of incoherent noise [1] and coherent deformations [3] as well as when both are present simultaneously [5]. The self-dual criticality can be viewed, in its own right, as a quantum parent state of the Nishimori criticality, which maintains the self-duality. It is interesting that in the language of the non-interacting fermion description of the KW self-dual

point this noise amounts to an interaction amongst the Majorana fermions during the crossover, while the two endpoints of the RG flow, the ultraviolet KW self-dual as well as the infrared Nishimori critical point, are both described in terms of *non-interacting* fermion systems.

Relationship with measurements performed on quantum critical ground states

The type of (1+1)D systems we discuss in the present paper belong to the setups appearing in the context of measurement induced phase transitions (MIPT) in deep 1D quantum circuits [71–74, 104, 105, 144, 145]. The systems we discuss are a particular (*e*- and *m*-) measurement-only [146] version of those, that surround the key question of weak self-duality symmetry, and which we write in the formulation of the mixed state of Eq. 2 in 2D space. In these setups measurements are performed on the 2D bulk spacetime of the quantum circuit. In such a circuit, including at the MIPT, the 2D bulk lacks space and time translational invariance in a fixed quantum trajectory. Only observables averaged over quantum trajectories (measurement outcomes) are described by (rather rich) non-unitary “random” CFTs. Examples are the self-dual and the Nishimori critical points discussed in this paper. The quantum state at the final time (the boundary) of the circuit is described by boundary critical properties of this “random” non-unitary bulk CFT [dictated by a particular scale-(and conformally)-invariant boundary condition].

This setup should be contrasted with another (technically more tractable) type of measurement setups that has been discussed in the more recent literature, where measurements are performed on a quantum critical ground state of a 1D translationally invariant critical Hamiltonian of a unitary (1+1)D CFT including, e.g., a gapless Luttinger liquid [147] or a critical transverse field Ising model in the first examples discussed, with natural generalizations to higher dimensional analogs (see, e.g., [7, 148]). When formulated in path integral language in (1+1)D spacetime [147], the quantum critical ground state is generated at the imaginary time $\tau = 0$ time-slice by an infinite imaginary time evolution from infinity with the unitary CFT Hamiltonian. Measurements are performed only at this $\tau = 0$ time-slice, representing a line-defect in (1+1)D space time. Away from the defect line, the 2D bulk of spacetime is completely translationally invariant. There are a number of versions of this setup, including e.g. those discussed in [147, 149–155] to briefly mention only a small subset. In many cases, including those where uniform measurement outcomes are postselected, the defect is described by a unitary defect/boundary CFT (bulk and defect/boundary are unitary). In cases where no uniform postselection (or bias) of measurement outcomes on the quantum critical ground state is performed, a defect can appear that itself needs to be described by non-unitary (‘random’) “measurement-dominated” defect/boundary fixed point CFT (exhibiting scaling behavior whose richness is qualitatively similar to that exhibited at general MITPs and by the systems discussed in the paper at hand). Examples of this are provided, e.g., in [155].

Connection to decoherence transitions of the toric code

Our phase diagram, parametrized by a measurement angle θ , describes the maximal decoherence limit of the toric code phase diagram of Ref. [6] which discusses a weak measurement / imperfect teleportation / Pauli noise channel, whose theory is described, as mentioned, by the symmetry class D NLSM with target space $SO(2N)/U(N)$ with theta term in the ($N \rightarrow 1$)-replica limit. The RG flow, revealed in our work here, shows that the weak self-dual critical state of the projectively measured toric code immediately flows to the Nishimori critical lines when the measurement strength is moved away from the projective limit (and turned into a weak measurement).

Previously, an ($N \rightarrow 0$)-replica limit was discussed in randomly deforming the toric code [156], while the ($N = 2$)-replica case was discussed more recently in Refs. [7, 58, 62, 70, 122]. These different replica limits all result in fundamentally distinct universality classes, pointing to the necessity to study the device-relevant ($N \rightarrow 1$)-replica limit of Born-measurement induced randomness in its own right (and despite its significant numerical effort) for any decoherence channel of interest.

Non-unitary measurement-based quantum computation

On a conceptual level, one way to think about the relation between bulk and boundary states is within the framework of measurement-based quantum computation (MBQC) [75, 76]. There, a 2D bulk cluster state serves as a (short-range) entanglement resource for a deep (1 + 1)D quantum circuit – propagating along one the two space dimensions instead of a real time dimension [82–86] – to prepare (compute) a nontrivial (1+1)D quantum state. The universality of MBQC guarantees that any *pure* state can be prepared, in this way, at the boundary of a cluster state by an effective *deterministic* (1+1)D unitary circuit with sufficient space resource and classical communication. What we discuss here is a seemingly very different setting with an effective circuit that is *probabilistic* non-unitary [88, 89] and leads to a *mixed* state [3, 4, 33, 131]. But if one thinks of MBQC as a measurement-based approach to implement conventional unitary state preparation (quantum annealing [157]), then one can cast our setting as a generalization of MBQC to non-unitary state preparation. This in turn points to a much broader application landscape of MBQC, as one can now imagine to prepare entangled mixed-states of matter that have no counterpart in the pure-state framework.

Outlook

Decoding

When decoding is employed and a conditional unitary based on the bulk classical bits (measurement records) is applied to the boundary quantum state, one can trace out the

bulk leaving a stand-alone boundary quantum state. An *optimal* decoder is one that can correct the whole SW-SSB phase at $t > \pi/8$ with glassy long-range order into an SSB phase with long-range order. Such a decoder would leave the KW self-dual critical location invariant, and could possibly preserve the self-duality at the transition point, turning our weak self-dual criticality into a standalone $(1 + 1)$ D mixed state: $\rho_Q = \sum_{em} U(em) |\psi(em)\rangle \langle \psi(em)|_Q U(em)^\dagger$, which should be amenable to near-term experimental probe [5].

Higher dimensions & Kitaev spin liquids

Moving onto higher dimensions, it is well-known that the 3D Ising criticality is *not* self-dual, but can rather be dualized to the 3D classical gauge theory [13]. However, the fermion perspective points to another potential generalization in three dimensions: a Majorana translation symmetric model with random vortex disorder. This could potentially be realized in cleverly designed 3D Kitaev spin liquids [158–160]. It is worth noting that a randomized version of monitored Kitaev spin liquids [161–163] is also closely related to the Floquet code of Hastings and Haah [164] – a new family of dynamical quantum error correcting codes [78, 165]. This points to another possible application of our duality-enriched mixed-state quantum criticality, to engineer the thresholds of dynamical quantum error correcting codes.

Generalized symmetries

Another versatile direction is to explore systematically a weak-symmetry generalization [7, 8, 67, 69, 70] of the more generic non-invertible or categorical symmetries [16, 17, 19,

21–25], when a quantum theory is subjected to decoherence. On the other hand, our self-dual decoherence could be generalized to more generic quantum error correction codes enriched with duality [166], or gauge theory with matter as for the (good) qLDPC codes [167].

DATA AVAILABILITY

The numerical data shown in the figures and the data for sweeping the phase diagram are available on Zenodo [168].

ACKNOWLEDGMENTS

GYZ would like to especially thank Samuel Garratt for inspiring discussions on the preparation of $(1 + 1)$ D critical states, as well as Shang-Qiang Ning and Chenjie Wang for discussions of the categorical symmetry and quantum anomaly. The authors would like to thank Malte Pütz for helpful discussions on the numerics of Nishimori criticality, to be published in a joint work [42]. AWWL thanks Chao-Ming Jian for collaboration on several previous works in the area of quantum circuits of non-interacting fermions. GYZ acknowledge the support by the start-up fund from HKUST(GZ). ST acknowledges partial funding from the Deutsche Forschungsgemeinschaft (DFG, German Research Foundation) under Germany’s Excellence Strategy – Cluster of Excellence Matter and Light for Quantum Computing (ML4Q) EXC 2004/1 – 390534769 and within the CRC network TR 183 (Project Grant No. 277101999) as part of subproject B01. R.V. acknowledges partial support from the US Department of Energy, Office of Science, Basic Energy Sciences, under award No. DE-SC0023999.

-
- [1] E. Dennis, A. Kitaev, A. Landahl, and J. Preskill, Topological quantum memory, *Journal of Mathematical Physics* **43**, 4452 (2002).
 - [2] H. Nishimori, Internal Energy, Specific Heat and Correlation Function of the Bond-Random Ising Model, *Progress of Theoretical Physics* **66**, 1169 (1981).
 - [3] G.-Y. Zhu, N. Tantivasadakarn, A. Vishwanath, S. Trebst, and R. Verresen, Nishimori’s Cat: Stable Long-Range Entanglement from Finite-Depth Unitaries and Weak Measurements, *Phys. Rev. Lett.* **131**, 200201 (2023).
 - [4] J. Y. Lee, W. Ji, Z. Bi, and M. P. A. Fisher, Measurement-Prepared Quantum Criticality: from Ising model to gauge theory, and beyond, (2022), [arXiv:2208.11699](https://arxiv.org/abs/2208.11699).
 - [5] E. H. Chen, G.-Y. Zhu, R. Verresen, A. Seif, E. Bäumer, D. Layden, N. Tantivasadakarn, G. Zhu, S. Sheldon, A. Vishwanath, S. Trebst, and A. Kandala, Nishimori transition across the error threshold for constant-depth quantum circuits, *Nature Physics* **21**, 161 (2025).
 - [6] F. Eckstein, B. Han, S. Trebst, and G.-Y. Zhu, Robust Teleportation of a Surface Code and Cascade of Topological Quantum Phase Transitions, *PRX Quantum* **5**, 040313 (2024).
 - [7] J. Y. Lee, C.-M. Jian, and C. Xu, Quantum Criticality Under Decoherence or Weak Measurement, *PRX Quantum* **4**, 030317 (2023).
 - [8] P. Sala, S. Gopalakrishnan, M. Oshikawa, and Y. You, Spontaneous strong symmetry breaking in open systems: Purification perspective, *Phys. Rev. B* **110**, 155150 (2024).
 - [9] L. A. Lessa, R. Ma, J.-H. Zhang, Z. Bi, M. Cheng, and C. Wang, Strong-to-Weak Spontaneous Symmetry Breaking in Mixed Quantum States, [arXiv:2405.03639](https://arxiv.org/abs/2405.03639).
 - [10] H. A. Kramers and G. H. Wannier, Statistics of the Two-Dimensional Ferromagnet. Part I, *Phys. Rev.* **60**, 252 (1941).
 - [11] I. A. Gruzberg, N. Read, and A. W. W. Ludwig, Random-bond Ising model in two dimensions: The Nishimori line and supersymmetry, *Phys. Rev. B* **63**, 104422 (2001).
 - [12] F. Merz and J. T. Chalker, Negative scaling dimensions and conformal invariance at the Nishimori point in the $\pm J$ random-bond Ising model, *Phys. Rev. B* **66**, 054413 (2002).
 - [13] F. J. Wegner, Duality in Generalized Ising Models and Phase Transitions without Local Order Parameters, *Journal of Mathematical Physics* **12**, 2259 (1971).

- [14] G. 't Hooft, On the phase transition towards permanent quark confinement, *Nuclear Physics B* **138**, 1 (1978).
- [15] E. Fradkin and S. H. Shenker, Phase diagrams of lattice gauge theories with Higgs fields, *Phys. Rev. D* **19**, 3682 (1979).
- [16] W. Ji and X.-G. Wen, Categorical symmetry and noninvertible anomaly in symmetry-breaking and topological phase transitions, *Phys. Rev. Res.* **2**, 033417 (2020).
- [17] A. Antinucci, F. Benini, C. Copetti, G. Galati, and G. Rizi, Anomalies of non-invertible self-duality symmetries: fractionalization and gauging, [arXiv:2308.11707](https://arxiv.org/abs/2308.11707).
- [18] A. Apte, C. Córdova, and H. T. Lam, Obstructions to gapped phases from noninvertible symmetries, *Phys. Rev. B* **108**, 045134 (2023).
- [19] Y.-H. Lin, M. Okada, S. Seifnashri, and Y. Tachikawa, Asymptotic density of states in 2d CFTs with non-invertible symmetries, *Journal of High Energy Physics* **2023**, 1 (2023).
- [20] N. Tantivasadakarn, R. Thorngren, A. Vishwanath, and R. Verresen, Long-Range Entanglement from Measuring Symmetry-Protected Topological Phases, *Phys. Rev. X* **14**, 021040 (2024).
- [21] N. Seiberg and S.-H. Shao, Majorana chain and Ising model - (non-invertible) translations, anomalies, and emanant symmetries, *SciPost Phys.* **16**, 064 (2024).
- [22] M. Okada and Y. Tachikawa, Noninvertible Symmetries Act Locally by Quantum Operations, *Phys. Rev. Lett.* **133**, 191602 (2024).
- [23] S.-Q. Ning, B.-B. Mao, and C. Wang, Building 1D lattice models with G -graded fusion category, *SciPost Phys.* **17**, 125 (2024).
- [24] L. Lootens, J. Fuchs, J. Haegeman, C. Schweigert, and F. Verstraete, Matrix product operator symmetries and intertwiners in string-nets with domain walls, *SciPost Phys.* **10**, 053 (2021).
- [25] D.-C. Lu, Z. Sun, and Y.-Z. You, Realizing triality and p -ality by lattice twisted gauging in $(1+1)d$ quantum spin systems, *SciPost Phys.* **17**, 136 (2024).
- [26] B. Buča and T. Prosen, A note on symmetry reductions of the Lindblad equation: transport in constrained open spin chains, *New Journal of Physics* **14**, 073007 (2012).
- [27] V. V. Albert and L. Jiang, Symmetries and conserved quantities in Lindblad master equations, *Phys. Rev. A* **89**, 022118 (2014).
- [28] S. Lieu, R. Belyansky, J. T. Young, R. Lundgren, V. V. Albert, and A. V. Gorshkov, Symmetry Breaking and Error Correction in Open Quantum Systems, *Phys. Rev. Lett.* **125**, 240405 (2020).
- [29] X. Chen, Z.-C. Gu, and X.-G. Wen, Local unitary transformation, long-range quantum entanglement, wave function renormalization, and topological order, *Phys. Rev. B* **82**, 155138 (2010).
- [30] A. Y. Kitaev, Fault-tolerant quantum computation by anyons, *Annals of Physics* **303**, 2 (2003).
- [31] D. M. Greenberger, M. A. Horne, and A. Zeilinger, Going Beyond Bell's Theorem, in *Bell's Theorem, Quantum Theory, and Conceptions of the Universe* (Kluwer, 1989) pp. 69–72, [arXiv:0712.0921](https://arxiv.org/abs/0712.0921).
- [32] H. J. Briegel and R. Raussendorf, Persistent Entanglement in Arrays of Interacting Particles, *Phys. Rev. Lett.* **86**, 910 (2001).
- [33] T.-C. Lu, Z. Zhang, S. Vijay, and T. H. Hsieh, Mixed-State Long-Range Order and Criticality from Measurement and Feedback, *PRX Quantum* **4**, 030318 (2023).
- [34] Y.-H. Chen and T. Grover, Separability Transitions in Topological States Induced by Local Decoherence, *Phys. Rev. Lett.* **132**, 170602 (2024).
- [35] A.-R. Negari, T. D. Ellison, and T. H. Hsieh, Spacetime Markov length: a diagnostic for fault tolerance via mixed-state phases, [arXiv:2412.00193](https://arxiv.org/abs/2412.00193).
- [36] R. Verresen, U. Borla, A. Vishwanath, S. Moroz, and R. Thorngren, Higgs Condensates are Symmetry-Protected Topological Phases: I. Discrete Symmetries, [arXiv:2211.01376](https://arxiv.org/abs/2211.01376).
- [37] X. Chen, Z.-X. Liu, and X.-G. Wen, Two-dimensional symmetry-protected topological orders and their protected gapless edge excitations, *Phys. Rev. B* **84**, 235141 (2011).
- [38] M. Levin and Z.-C. Gu, Braiding statistics approach to symmetry-protected topological phases, *Phys. Rev. B* **86**, 115109 (2012).
- [39] D. T. Stephen, D.-S. Wang, A. Prakash, T.-C. Wei, and R. Raussendorf, Computational Power of Symmetry-Protected Topological Phases, *Phys. Rev. Lett.* **119**, 010504 (2017).
- [40] J. B. Kogut, An introduction to lattice gauge theory and spin systems, *Rev. Mod. Phys.* **51**, 659 (1979).
- [41] I. S. Tupitsyn, A. Kitaev, N. V. Prokof'ev, and P. C. E. Stamp, Topological multicritical point in the phase diagram of the toric code model and three-dimensional lattice gauge Higgs model, *Phys. Rev. B* **82**, 085114 (2010).
- [42] M. Pütz, R. Vasseur, A. W. W. Ludwig, S. Trebst, and G.-Y. Zhu, to appear, (2025).
- [43] R. Verresen, N. Tantivasadakarn, and A. Vishwanath, Efficiently preparing Schrödinger's cat, fractons and non-Abelian topological order in quantum devices, (2021), [arXiv:2112.03061](https://arxiv.org/abs/2112.03061).
- [44] Strictly speaking, a cat state does not break the symmetry on the microscopic level, but we still relate such cat state to an SSB order, because it has the defining long-range correlation.
- [45] C. L. Henley, From classical to quantum dynamics at Rokhsar–Kivelson points, *Journal of Physics: Condensed Matter* **16**, S891 (2004).
- [46] E. Ardonne, P. Fendley, and E. Fradkin, Topological order and conformal quantum critical points, *Annals of Physics* **310**, 493 (2004).
- [47] C. Castelnovo, S. Trebst, and M. Troyer, Topological Order and Quantum Criticality, in *Understanding Quantum Phase Transitions* (Taylor & Francis, 2010) pp. 169–192, [arXiv:0912.3272](https://arxiv.org/abs/0912.3272).
- [48] F. Verstraete, M. M. Wolf, D. Perez-Garcia, and J. I. Cirac, Criticality, the Area Law, and the Computational Power of Projected Entangled Pair States, *Phys. Rev. Lett.* **96**, 220601 (2006).
- [49] A. Y. Kitaev, Unpaired Majorana fermions in quantum wires, *Physics-Uspekhi* **44**, 131 (2001).
- [50] R. Raussendorf, J. Harrington, and K. Goyal, Topological fault-tolerance in cluster state quantum computation, *New Journal of Physics* **9**, 199 (2007).
- [51] T.-C. Lu, L. A. Lessa, I. H. Kim, and T. H. Hsieh, Measurement as a Shortcut to Long-Range Entangled Quantum Matter, *PRX Quantum* **3**, 040337 (2022).
- [52] M. Iqbal, N. Tantivasadakarn, T. M. Gatterman, J. A. Gerber, K. Gilmore, D. Gresh, A. Hankin, N. Hewitt, C. V. Horst, M. Matheny, T. Mengle, B. Neyenhuis, A. Vishwanath, M. Foss-Feig, R. Verresen, and H. Dreyer, Topological Order from Measurements and Feed-Forward on a Trapped Ion Quantum Computer, (2023), [arXiv:2302.01917](https://arxiv.org/abs/2302.01917).
- [53] S. Bravyi, M. Englbrecht, R. König, and N. Peard, Correcting coherent errors with surface codes, *npj Quantum Information* **4**, 55 (2018).
- [54] J. K. Iverson and J. Preskill, Coherence in logical quantum channels, *New Journal of Physics* **22**, 073066 (2020).

- [55] F. Venn, J. Behrends, and B. Béri, Coherent-Error Threshold for Surface Codes from Majorana Delocalization, *Phys. Rev. Lett.* **131**, 060603 (2023).
- [56] P. Niroula, C. D. White, Q. Wang, S. Johri, D. Zhu, C. Monroe, C. Noel, and M. J. Gullans, Phase transition in magic with random quantum circuits, *Nature Physics* **20**, 1786 (2024).
- [57] J. Behrends, F. Venn, and B. Béri, Surface codes, quantum circuits, and entanglement phases, *Phys. Rev. Res.* **6**, 013137 (2024).
- [58] S. Lee and E.-G. Moon, Mixed-State Topological Order under Coherent Noises, [arXiv:2411.03441](https://arxiv.org/abs/2411.03441).
- [59] Z. Cheng, E. Huang, V. Khemani, M. J. Gullans, and M. Ippoliti, Emergent unitary designs for encoded qubits from coherent errors and syndrome measurements, [arXiv:2412.04414](https://arxiv.org/abs/2412.04414).
- [60] Y. Bao and S. Anand, Phases of decodability in the surface code with unitary errors, (2024), [arXiv:2411.05785](https://arxiv.org/abs/2411.05785).
- [61] G.-Y. Zhu and G.-M. Zhang, Gapless Coulomb State Emerging from a Self-Dual Topological Tensor-Network State, *Phys. Rev. Lett.* **122**, 176401 (2019).
- [62] Y.-H. Chen and T. Grover, Unconventional topological mixed-state transition and critical phase induced by self-dual coherent errors, *Phys. Rev. B* **110**, 125152 (2024).
- [63] A.-R. Negari, S. Sahu, and T. H. Hsieh, Measurement-induced phase transitions in the toric code, *Phys. Rev. B* **109**, 125148 (2024).
- [64] I. S. Tupitsyn, A. Kitaev, N. V. Prokof'ev, and P. C. E. Stamp, Topological multicritical point in the phase diagram of the toric code model and three-dimensional lattice gauge Higgs model, *Phys. Rev. B* **82**, 085114 (2010).
- [65] A. M. Somoza, P. Serna, and A. Nahum, Self-Dual Criticality in Three-Dimensional \mathbb{Z}_2 Gauge Theory with Matter, *Phys. Rev. X* **11**, 041008 (2021).
- [66] J. Haegeman, V. Zauner, N. Schuch, and F. Verstraete, Shadows of anyons and the entanglement structure of topological phases, *Nature Communications* **6**, 8284 (2015).
- [67] R. Ma and C. Wang, Average Symmetry-Protected Topological Phases, *Phys. Rev. X* **13**, 031016 (2023).
- [68] R. Ma, J.-H. Zhang, Z. Bi, M. Cheng, and C. Wang, Topological Phases with Average Symmetries: the Decohered, the Disordered, and the Intrinsic, [arXiv:2305.16399](https://arxiv.org/abs/2305.16399).
- [69] K. Su, N. Myerson-Jain, C. Wang, C.-M. Jian, and C. Xu, Higher-Form Symmetries under Weak Measurement, *Phys. Rev. Lett.* **132**, 200402 (2024).
- [70] C. Zhang, Y. Xu, J.-H. Zhang, C. Xu, Z. Bi, and Z.-X. Luo, Strong-to-weak spontaneous breaking of 1-form symmetry and intrinsically mixed topological order, [arXiv:2409.17530](https://arxiv.org/abs/2409.17530).
- [71] Y. Li, X. Chen, and M. P. A. Fisher, Quantum Zeno effect and the many-body entanglement transition, *Phys. Rev. B* **98**, 205136 (2018).
- [72] B. Skinner, J. Ruhman, and A. Nahum, Measurement-Induced Phase Transitions in the Dynamics of Entanglement, *Phys. Rev. X* **9**, 031009 (2019).
- [73] A. C. Potter and R. Vasseur, Entanglement Dynamics in Hybrid Quantum Circuits, in *Entanglement in Spin Chains*, edited by A. Bayat, S. Bose, and H. Johannesson (Springer International Publishing, Cham, 2022) pp. 211–249.
- [74] M. P. Fisher, V. Khemani, A. Nahum, and S. Vijay, Random Quantum Circuits, *Annual Review of Condensed Matter Physics* **14**, 335 (2023).
- [75] R. Raussendorf and H. J. Briegel, A One-Way Quantum Computer, *Phys. Rev. Lett.* **86**, 5188 (2001).
- [76] H. J. Briegel, D. E. Browne, W. Dür, R. Raussendorf, and M. Van den Nest, Measurement-based quantum computation, *Nature Physics* **5**, 19 (2009).
- [77] Otherwise, the final state can be viewed as first preparing a critical Ising state described by unitary CFT and then subjecting that state to uniformly post-selected measurement, which generally changes the entanglement structure [42, 149–152, 155].
- [78] D. Aasen, Z. Wang, and M. B. Hastings, Adiabatic paths of Hamiltonians, symmetries of topological order, and automorphism codes, *Phys. Rev. B* **106**, 085122 (2022).
- [79] L. Lootens, C. Delcamp, G. Ortiz, and F. Verstraete, Dualities in One-Dimensional Quantum Lattice Models: Symmetric Hamiltonians and Matrix Product Operator Intertwiners, *PRX Quantum* **4**, 020357 (2023).
- [80] The Paulis at the final time slice can be annihilated by acting a single layer of exactly the same Pauli gates to the final quantum state, making use of the measurement outcome.
- [81] Note that the final time β' takes half of its value in order to implement $\sqrt{M_X}$.
- [82] D. E. Browne, M. B. Elliott, S. T. Flammia, S. T. Merkel, A. Miyake, and A. J. Short, Phase transition of computational power in the resource states for one-way quantum computation, *New Journal of Physics* **10**, 023010 (2008).
- [83] Y. Bao, M. Block, and E. Altman, Finite-Time Teleportation Phase Transition in Random Quantum Circuits, *Phys. Rev. Lett.* **132**, 030401 (2024).
- [84] H. Liu, T. Zhou, and X. Chen, Measurement-induced entanglement transition in a two-dimensional shallow circuit, *Phys. Rev. B* **106**, 144311 (2022).
- [85] J. C. Napp, R. L. La Placa, A. M. Dalzell, F. G. S. L. Brandão, and A. W. Harrow, Efficient Classical Simulation of Random Shallow 2D Quantum Circuits, *Phys. Rev. X* **12**, 021021 (2022).
- [86] Google Quantum AI and Collaborators, Measurement-induced entanglement and teleportation on a noisy quantum processor, *Nature* **622**, 481 (2023).
- [87] C. H. Bennett, G. Brassard, C. Crépeau, R. Jozsa, A. Peres, and W. K. Wootters, Teleporting an unknown quantum state via dual classical and Einstein-Podolsky-Rosen channels, *Phys. Rev. Lett.* **70**, 1895 (1993).
- [88] D. Azses, J. Ruhman, and E. Sela, Nonunitary Gates Using Measurements Only, *Phys. Rev. Lett.* **133**, 260603 (2024).
- [89] H. Terashima and M. Ueda, Non-unitary Quantum Circuit, *International Journal of Quantum Information* **03**, 633 (2005).
- [90] L. P. Kadanoff and H. Ceva, Determination of an Operator Algebra for the Two-Dimensional Ising Model, *Phys. Rev. B* **3**, 3918 (1971).
- [91] V. Gurarie and A. W. W. Ludwig, Conformal field theory at central charge $c=0$ and two-dimensional critical systems with quenched disorder, in *From Fields to Strings: Circumnavigating Theoretical Physics* (World Scientific, 2005) pp. 1384–1440.
- [92] A. Zabalo, M. J. Gullans, J. H. Wilson, R. Vasseur, A. W. W. Ludwig, S. Gopalakrishnan, D. A. Huse, and J. H. Pixley, Operator Scaling Dimensions and Multifractality at Measurement-Induced Transitions, *Phys. Rev. Lett.* **128**, 050602 (2022).
- [93] A. Kumar, K. Aziz, A. Chakraborty, A. W. W. Ludwig, S. Gopalakrishnan, J. H. Pixley, and R. Vasseur, Boundary transfer matrix spectrum of measurement-induced transitions, *Phys. Rev. B* **109**, 014303 (2024).
- [94] V. Gurarie, Logarithmic operators in conformal field theory, *Nuclear Physics B* **410**, 535 (1993).
- [95] V. Gurarie, c -Theorem for disordered systems, *Nuclear Physics B* **546**, 765 (1999).

- [96] J. Cardy, Logarithmic conformal field theories as limits of ordinary CFTs and some physical applications, *Journal of Physics A: Mathematical and Theoretical* **46**, 494001 (2013).
- [97] T. Creutzig and D. Ridout, Logarithmic conformal field theory: beyond an introduction, *Journal of Physics A: Mathematical and Theoretical* **46**, 494006 (2013).
- [98] H. W. J. Blöte, J. L. Cardy, and M. P. Nightingale, Conformal invariance, the central charge, and universal finite-size amplitudes at criticality, *Phys. Rev. Lett.* **56**, 742 (1986).
- [99] A. Nahum and B. Skinner, Entanglement and dynamics of diffusion-annihilation processes with Majorana defects, *Phys. Rev. Res.* **2**, 023288 (2020).
- [100] I.e., fermion parity measurements of the kind employed in [101] and [119], where the second reference discussed only the case where unitary gates are also always present in addition to fermion parity measurements.
- [101] M. Fava, L. Piroli, T. Swann, D. Bernard, and A. Nahum, Nonlinear Sigma Models for Monitored Dynamics of Free Fermions, *Phys. Rev. X* **13**, 041045 (2023).
- [102] K. Jacobs and D. A. Steck, A straightforward introduction to continuous quantum measurement, *Contemporary Physics* **47**, 279 (2006).
- [103] G. Kells, D. Meidan, and A. Romito, Topological transitions in weakly monitored free fermions, *SciPost Phys.* **14**, 031 (2023).
- [104] C.-M. Jian, Y.-Z. You, R. Vasseur, and A. W. W. Ludwig, Measurement-induced criticality in random quantum circuits, *Phys. Rev. B* **101**, 104302 (2020).
- [105] Y. Bao, S. Choi, and E. Altman, Theory of the phase transition in random unitary circuits with measurements, *Phys. Rev. B* **101**, 104301 (2020).
- [106] N. Read and A. W. W. Ludwig, Absence of a metallic phase in random-bond Ising models in two dimensions: Applications to disordered superconductors and paired quantum Hall states, *Phys. Rev. B* **63**, 024404 (2000).
- [107] J. T. Chalker, N. Read, V. Kagalovsky, B. Horovitz, Y. Avishai, and A. W. W. Ludwig, Thermal metal in network models of a disordered two-dimensional superconductor, *Phys. Rev. B* **65**, 012506 (2001).
- [108] C.-M. Jian, B. Bauer, A. Keselman, and A. W. W. Ludwig, Criticality and entanglement in nonunitary quantum circuits and tensor networks of noninteracting fermions, *Phys. Rev. B* **106**, 134206 (2022).
- [109] A. Altland and M. R. Zirnbauer, Nonstandard symmetry classes in mesoscopic normal-superconducting hybrid structures, *Phys. Rev. B* **55**, 1142 (1997).
- [110] J. T. Chalker and P. D. Coddington, Percolation, quantum tunnelling and the integer Hall effect, *Journal of Physics C: Solid State Physics* **21**, 2665 (1988).
- [111] The “surrounding lattice”, whose sites are the midpoints of the links in Fig. 2(c), and on whose bonds the Majorana fermions propagate, is not drawn explicitly drawn in Fig. 2(d).
- [112] Besides an actual spin-glass phase appearing in the phase diagram of the RBIM at *zero temperature* (using the conventional classical statistical mechanics model coordinates of the phase diagram, which are temperature and negative exchange coupling disorder), which we do not address in the present work.
- [113] Related to each other by Kramers-Wannier duality.
- [114] S. Cho and M. P. A. Fisher, Criticality in the two-dimensional random-bond Ising model, *Phys. Rev. B* **55**, 1025 (1997).
- [115] T. Wang, Z. Pan, T. Ohtsuki, I. A. Gruzberg, and R. Shindou, Multicriticality of two-dimensional class-D disordered topological superconductors, *Phys. Rev. B* **104**, 184201 (2021).
- [116] A. W. W. Ludwig, Topological phases: classification of topological insulators and superconductors of non-interacting fermions, and beyond, *Physica Scripta* **2016**, 014001 (2015).
- [117] M. R. Zirnbauer, Riemannian symmetric superspaces and their origin in random-matrix theory, *Journal of Mathematical Physics* **37**, 4986 (1996).
- [118] S. Ryu, A. P. Schnyder, A. Furusaki, and A. W. W. Ludwig, Topological insulators and superconductors: tenfold way and dimensional hierarchy, *New Journal of Physics* **12**, 065010 (2010).
- [119] C.-M. Jian, H. Shapourian, B. Bauer, and A. W. W. Ludwig, Measurement-induced entanglement transitions in quantum circuits of non-interacting fermions: Born-rule versus forced measurements, (2023), [arXiv:2302.09094](https://arxiv.org/abs/2302.09094).
- [120] B. Schumacher and M. A. Nielsen, Quantum data processing and error correction, *Phys. Rev. A* **54**, 2629 (1996).
- [121] M. J. Gullans and D. A. Huse, Scalable Probes of Measurement-Induced Criticality, *Phys. Rev. Lett.* **125**, 070606 (2020).
- [122] R. Fan, Y. Bao, E. Altman, and A. Vishwanath, Diagnostics of Mixed-State Topological Order and Breakdown of Quantum Memory, *PRX Quantum* **5**, 020343 (2024).
- [123] Z.-M. Huang, L. Colmenarez, M. Müller, and S. Diehl, Coherent information as a mixed-state topological order parameter of fermions, [arXiv:2412.12279](https://arxiv.org/abs/2412.12279).
- [124] C. Nayak, S. H. Simon, A. Stern, M. Freedman, and S. Das Sarma, Non-Abelian anyons and topological quantum computation, *Rev. Mod. Phys.* **80**, 1083 (2008).
- [125] F. Barratt, U. Agrawal, A. C. Potter, S. Gopalakrishnan, and R. Vasseur, Transitions in the Learnability of Global Charges from Local Measurements, *Phys. Rev. Lett.* **129**, 200602 (2022).
- [126] M. Ippoliti and V. Khemani, Learnability Transitions in Monitored Quantum Dynamics via Eavesdropper’s Classical Shadows, *PRX Quantum* **5**, 020304 (2024).
- [127] The Rényi entropies, on the other hand, cannot be simply decomposed but rather involves a n -replica average of the n -th order purity: $S_{(n)}(\rho) = \frac{1}{1-n} \ln \text{tr} \rho^n = \frac{1}{1-n} \ln \sum_{em} P(em)^n e^{(1-n)S_n(em)}$.
- [128] A. Honecker, M. Picco, and P. Pujol, Universality Class of the Nishimori Point in the 2D $\pm J$ Random-Bond Ising Model, *Phys. Rev. Lett.* **87**, 047201 (2001).
- [129] M. Picco, A. Honecker, and P. Pujol, Strong disorder fixed points in the two-dimensional random-bond Ising model, *Journal of Statistical Mechanics: Theory and Experiment* **2006**, P09006 (2006).
- [130] Y. Li, R. Vasseur, M. P. A. Fisher, and A. W. W. Ludwig, Statistical mechanics model for Clifford random tensor networks and monitored quantum circuits, *Phys. Rev. B* **109**, 174307 (2024).
- [131] S. Sang and T. H. Hsieh, Stability of mixed-state quantum phases via finite Markov length, [arXiv:2404.07251](https://arxiv.org/abs/2404.07251).
- [132] C. Castelnovo and C. Chamon, Entanglement and topological entropy of the toric code at finite temperature, *Phys. Rev. B* **76**, 184442 (2007).
- [133] M. B. Hastings, Topological Order at Nonzero Temperature, *Phys. Rev. Lett.* **107**, 210501 (2011).
- [134] Y. Bao, R. Fan, A. Vishwanath, and E. Altman, Mixed-state topological order and the errorfield double formulation of decoherence-induced transitions, [arXiv:2301.05687](https://arxiv.org/abs/2301.05687).
- [135] Y. Guo and S. Yang, Locally purified density operators for noisy quantum circuits, *Chinese Physics Letters* **41**, 120302 (2024).

- [136] M.-D. Choi, Completely positive linear maps on complex matrices, *Linear Algebra and its Applications* **10**, 285 (1975).
- [137] A. Jamiolkowski, Linear transformations which preserve trace and positive semidefiniteness of operators, *Reports on Mathematical Physics* **3**, 275 (1972).
- [138] Note that we supplement the finite-size random tensor network computation by a Markov chain Monte Carlo sampling as in Ref. [3].
- [139] F. Merz and J. T. Chalker, Two-dimensional random-bond Ising model, free fermions, and the network model, *Phys. Rev. B* **65**, 054425 (2002).
- [140] J. C. Lessa and S. L. A. de Queiroz, Properties of the multicritical point of $\pm J$ Ising spin glasses on the square lattice, *Phys. Rev. B* **74**, 134424 (2006).
- [141] Y. Sasagawa, H. Ueda, J. Genzor, A. Gendiar, and T. Nishino, Entanglement entropy on the boundary of the square-lattice $\pm J$ Ising model, *Journal of the Physical Society of Japan* **89**, 114005 (2020).
- [142] S. V. Isakov, P. Fendley, A. W. W. Ludwig, S. Trebst, and M. Troyer, Dynamics at and near conformal quantum critical points, *Phys. Rev. B* **83**, 125114 (2011).
- [143] In the periodic boundary condition, $\text{KW} |\psi\rangle|_{\gamma=\infty} = \frac{1+\prod_j X_j}{2} |\psi\rangle|_{\gamma=\infty}$, the self-dual state is invariant locally but experiences a global parity projector, which can be verified in the MPO form of the symmetry in Fig. 2a. In a twisted boundary condition it becomes the odd parity projector.
- [144] M. J. Gullans and D. A. Huse, Dynamical Purification Phase Transition Induced by Quantum Measurements, *Phys. Rev. X* **10**, 041020 (2020).
- [145] A. Zabalo, M. J. Gullans, J. H. Wilson, S. Gopalakrishnan, D. A. Huse, and J. H. Pixley, Critical properties of the measurement-induced transition in random quantum circuits, *Phys. Rev. B* **101**, 060301 (2020).
- [146] M. Ippoliti, M. J. Gullans, S. Gopalakrishnan, D. A. Huse, and V. Khemani, Entanglement Phase Transitions in Measurement-Only Dynamics, *Phys. Rev. X* **11**, 011030 (2021).
- [147] S. J. Garratt, Z. Weinstein, and E. Altman, Measurements Conspire Nonlocally to Restructure Critical Quantum States, *Phys. Rev. X* **13**, 021026 (2023).
- [148] K. Baweja, D. J. Luitz, and S. J. Garratt, *Post-measurement Quantum Monte Carlo* (2024), [arXiv:2410.13844](https://arxiv.org/abs/2410.13844) [cond-mat.stat-mech].
- [149] Z. Weinstein, R. Sajith, E. Altman, and S. J. Garratt, Non-locality and entanglement in measured critical quantum Ising chains, *Phys. Rev. B* **107**, 245132 (2023).
- [150] S. Murciano, P. Sala, Y. Liu, R. S. K. Mong, and J. Alicea, Measurement-Altered Ising Quantum Criticality, *Phys. Rev. X* **13**, 041042 (2023).
- [151] Z. Yang, D. Mao, and C.-M. Jian, Entanglement in a one-dimensional critical state after measurements, *Phys. Rev. B* **108**, 165120 (2023).
- [152] Y. Zou, S. Sang, and T. H. Hsieh, Channeling Quantum Criticality, *Phys. Rev. Lett.* **130**, 250403 (2023).
- [153] P. Sala, S. Murciano, Y. Liu, and J. Alicea, Quantum Criticality Under Imperfect Teleportation, *PRX Quantum* **5**, 030307 (2024).
- [154] Y. Liu, S. Murciano, D. F. Mross, and J. Alicea, *Boundary transitions from a single round of measurements on gapless quantum states* (2024), [arXiv:2412.07830](https://arxiv.org/abs/2412.07830) [quant-ph].
- [155] R. A. Patil and A. W. W. Ludwig, Highly complex novel critical behavior from the intrinsic randomness of quantum mechanical measurements on critical ground states – a controlled renormalization group analysis, [arXiv:2409.02107](https://arxiv.org/abs/2409.02107).
- [156] D. I. Tsomokos, T. J. Osborne, and C. Castelnovo, Interplay of topological order and spin glassiness in the toric code under random magnetic fields, *Phys. Rev. B* **83**, 075124 (2011).
- [157] T. Kadowaki and H. Nishimori, Quantum annealing in the transverse Ising model, *Phys. Rev. E* **58**, 5355 (1998).
- [158] A. Kitaev, Anyons in an exactly solved model and beyond, *Annals of Physics* **321**, 2 (2006).
- [159] K. O’Brien, M. Hermanns, and S. Trebst, Classification of gapless \mathbb{Z}_2 spin liquids in three-dimensional Kitaev models, *Phys. Rev. B* **93**, 085101 (2016).
- [160] T. Eschmann, P. A. Mishchenko, K. O’Brien, T. A. Bojesen, Y. Kato, M. Hermanns, Y. Motome, and S. Trebst, Thermodynamic classification of three-dimensional Kitaev spin liquids, *Phys. Rev. B* **102**, 075125 (2020).
- [161] G.-Y. Zhu, N. Tantivasadakarn, and S. Trebst, Structured volume-law entanglement in an interacting, monitored Majorana spin liquid, *Phys. Rev. Res.* **6**, L042063 (2024).
- [162] G.-Y. Zhu and S. Trebst, Qubit fractionalization and emergent Majorana liquid in the honeycomb Floquet code induced by coherent errors and weak measurements, (2023), [arXiv:2311.08450](https://arxiv.org/abs/2311.08450).
- [163] K. Klocke, D. Simm, G.-Y. Zhu, S. Trebst, and M. Buchhold, Entanglement dynamics in monitored Kitaev circuits: loop models, symmetry classification, and quantum Lifshitz scaling, (2024), [arXiv:2409.02171](https://arxiv.org/abs/2409.02171).
- [164] M. B. Hastings and J. Haah, Dynamically Generated Logical Qubits, *Quantum* **5**, 564 (2021).
- [165] A. Dua, N. Tantivasadakarn, J. Sullivan, and T. D. Ellison, Engineering 3D Floquet Codes by Rewinding, *PRX Quantum* **5**, 020305 (2024).
- [166] K. Su, Z. Yang, and C.-M. Jian, Tapestry of dualities in decohered quantum error correction codes, *Phys. Rev. B* **110**, 085158 (2024).
- [167] T. Rakovszky and V. Khemani, The Physics of (good) LDPC Codes I. Gauging and dualities, [arXiv:2310.16032](https://arxiv.org/abs/2310.16032).
- [168] Q. Wang, R. Vasseur, S. Trebst, A. W. W. Ludwig, and G.-Y. Zhu, Data for “Decoherence-induced self-dual criticality in topological states of matter” [10.5281/zenodo.14876155](https://zenodo.org/record/14876155) (2025).

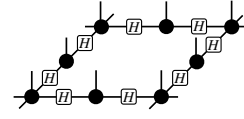
CONTENTS

| | | | |
|--|----|---|----|
| | | Second Rényi coherent information | 27 |
| | | Nishimori criticality in the maximally noisy limit | 27 |
| II. Model | 3 | B. Born-average Rényi entropies | 28 |
| A. Protocol: preparation and decoherence | 3 | C. Comparison with continuous weak measurement | 28 |
| B. Z_2 gauge perspective for the intermediate state | 4 | Bimodal discrete weak measurement | 28 |
| C. Tensor network state representation | 4 | Gaussian continuous weak measurement | 29 |
| D. Symmetries | 5 | D. Central charge of Ising+ | 29 |
| E. Mixed state dynamics | 5 | E. Supplementary data for finite-size data collapse | 30 |
| III. Equivalent Model Representations | 5 | | |
| A. (1+1)D monitored quantum circuit | 5 | | |
| Clean Ising in a uniformly post-selected trajectory | 5 | | |
| Measurement-induced random trajectories | 7 | | |
| Non-unitary measurement-based quantum computation | 7 | | |
| B. 2D Classical statistical model | 7 | | |
| Free energy and central charge | 8 | | |
| C. (1+1)D monitored Majorana circuit | 8 | | |
| D. (2+1)D Chalker-Coddington network model | 8 | | |
| Relationship with previous work | 9 | | |
| IV. The self-dual critical state | 10 | | |
| A. Coherent information | 10 | | |
| B. Bulk Shannon entropy | 12 | | |
| Lyapunov spectrum | 12 | | |
| C. Boundary entanglement entropy | 13 | | |
| V. Mixed-state phase diagram and RG flows | 14 | | |
| A. Breaking self-duality by measurement noise | 14 | | |
| RG flow | 15 | | |
| B. Breaking self-duality by deformation | 16 | | |
| C. Strong to weak self-dual symmetry | 17 | | |
| VI. Discussion and outlook | 17 | | |
| Summary of RG flows | 17 | | |
| Relationship with measurements performed on quantum critical ground states | 18 | | |
| Connection to decoherence transitions of the toric code | 18 | | |
| Non-unitary measurement-based quantum computation | 18 | | |
| Outlook | 18 | | |
| Decoding | 18 | | |
| Higher dimensions & Kitaev spin liquids | 19 | | |
| Generalized symmetries | 19 | | |
| Data availability | 19 | | |
| Acknowledgments | 19 | | |
| References | 19 | | |
| A. Technical details | 24 | | |
| 1. Derivation for the random tensor network state | 24 | | |
| 2. Cylindrical boundary conditions | 24 | | |
| 3. Lyapunov spectrum | 25 | | |
| 4. Derivation for the noisy Choi state | 27 | | |
| Choi state as a tensor network state | 27 | | |

Appendix A: Technical details

1. Derivation for the random tensor network state

Prior to the measurements, the cluster state can be written as a tensor network:



which shows one plaquette as a unit-cell of the tensor network state. Each vertex is a diagonal delta tensor, originating from the initial $|+\rangle$ state of each qubit, and each bond is attached a 2-by-2 Hadamard matrix, which originates from the 4-by-4 CZ gate matrix: $\text{diag}(CZ) = [1, 1, 1, -1] \Leftrightarrow H = [1, 1; 1, -1]$. When a site qubit is measured in the X basis, the physical leg is terminated, and a Pauli Z is injected to the vertex if the measurement outcome is negative: $X = -1$. When a bond qubit is measured in the rotated basis, the physical leg is terminated, leaving a Boltzmann weight in the form of a 2-by-2 matrix associated with the bond

$$\begin{array}{c}
 i \\
 \bullet \\
 | \\
 \bullet \\
 | \\
 \bullet \\
 j
 \end{array}
 \begin{array}{c}
 \text{---} \text{Z} \text{---} \\
 | \\
 \text{---} \text{H} \text{---} \\
 | \\
 \text{---} \text{H} \text{---} \\
 | \\
 \text{---} \text{Z} \text{---}
 \end{array}
 \propto e^{s \frac{\beta}{2} Z Z_i} ,
 \quad
 \begin{array}{c}
 \text{---} \text{Z} \text{---} \\
 | \\
 \text{---} \text{H} \text{---} \\
 | \\
 \text{---} \text{H} \text{---} \\
 | \\
 \text{---} \text{Z} \text{---}
 \end{array}
 \propto e^{\frac{\beta}{2} X \cdot X^{1-s}} .
 \tag{A1}$$

2. Cylindrical boundary conditions

Here we discuss the boundary condition of the statistical model in the fermion representation when we place the 2D quantum state on a cylinder, i.e. implementing a periodic boundary condition along the X direction. If the measurement outcomes are post-selected to be positive, the statistical model is a clean 1+1D Ising model in the periodic boundary condition. And when the boundary term is twisted to be antiperiodic boundary condition, it excites an Ising primary field that costs energy. Nevertheless, in the presence of random bond disorder which breaks the translation symmetry, it

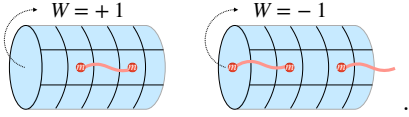
is less clear to determine the periodic or anti-periodic boundary condition by directly looking at a given bond. Essentially, the boundary condition is related to the global flux pumped to the cylinder, which is still well defined in the disordered system. Consider the generators of the dynamics by taking into account a random bond, which under Jordan-Wigner transformation becomes

$$\begin{aligned} s_{x,y} Z_x Z_{x+1} &= s_{x,y} i \gamma_{2x} \gamma_{2x+1}, \\ s_{x,y+\frac{1}{2}} X_x &= s_{x,y+\frac{1}{2}} i \gamma_{2x-1} \gamma_{2x}, \end{aligned} \quad (\text{A2})$$

where at the boundary $\gamma_{2L_x+1} = -P\gamma_1$. Here there are two independent global quantum numbers

$$\begin{aligned} W &= \prod_{x,y=1} s_{x,y} = \pm 1, \\ P &= \prod_{j=1}^{L_x} X_j = \prod_{j=1}^{L_x} i \gamma_{2j-1} \gamma_{2j} = \pm 1, \end{aligned} \quad (\text{A3})$$

where W determines the global flux pumped through the cylinder being 0 or π , and P specifies the parity of the spin or the fermion. A schematic of the two global fluxes under the same em configuration is illustrated below



In the clean 1+1D Ising, the vacuum state lies in $W = +1, P = +1$ and the lowest excited Ising primary field lies at $W = +1, P = -1$, which has a dual counterpart, i.e. a domain wall excitation that twists the boundary condition $W = -1, P = +1$ with the same scaling dimension $1/8$. This degeneracy is related to the exact zero modes when the fermion is placed at periodic boundary condition such that its momentum can take 0 value. In the disordered system, the global flux that the fermion experiences is determined by $-WP$ taking into account the flux induced by the random bond disorder and the opposite of the fermion parity. Once the boundary condition is fixed, the state is further divided into the two sectors determined by P . Technically, we will perform the Born measurements to get the Born ensemble as a grand canonical ensemble of the global flux, and then we divide the ensemble according to $W = \pm 1$, and fill the ‘‘Fermi sea’’ of the single-particle fermion eigenenergy levels to get the many-body state energy of the even fermion parity $\tilde{P} = +1$ in the eigen-fermion basis (caution that the fermion parity of the eigenmodes could differ from the original fermion modes [139] by a fixed sign). Then we can generate the many-body Lyapunov spectrum of even parity by increasing the double number of eigen-fermion modes, and that of the odd parity $\tilde{P} = -1$ by increasing an odd number of eigen-fermion modes.

3. Lyapunov spectrum

Akin to the numerical approach to Chalker-Coddington network models in Ref. [139], we evolve the (1+1)D quantum chain with $2L_x$ Majorana fermions up to long times $L_y \gg L_x$, which relaxes to a ‘‘steady’’ state, getting rid of the temporal boundary effect. In order to extract the universal *bulk* information, we discard the initial dynamics at early times, and perform statistics for the norm change of each fermion mode from now on. After a layer of gates, L_x independent, normalized fermion modes linearly evolve to a set of un-normalized fermion modes, whose norms change by a factor r_n for $n = 1, \dots, L_x$ in descending order. Numerically, r_n is the diagonal element of the R matrix after the QR decomposition for a layer of gates (which can be further decomposed to smaller chunk of gates in order to suppress the rounding error when L_x is large). r_n can be treated as a random variable that fluctuates as time evolves. The typical average $\epsilon_n = -\ln r_n$ for $n = 1, \dots, L_x$ can be interpreted as the single-particle fermion energies of the (1+1)D quantum chain. Back to the second quantization picture, the many-body energies, or the Lyapunov exponents are

$$E_m = \frac{1}{2} \sum_{n=1}^{L_x} \nu_n \epsilon_n \propto \frac{2\pi}{L_x} \left(\Delta_m - \frac{c_{\text{Casimir}}}{12} \right) + \dots, \quad (\text{A4})$$

where $\nu_n = \pm 1$ specifies the parity of the n -th eigenfermion mode, and by enumerating all the possibilities we have $m = 1, \dots, 2^{L_x}$ many-body eigen-energy levels. Here the many-body levels can be further divided according to the global fermion parity.

The spacetime bulk of the evolution as a transfer matrix converges to $\prod_y M(y) = \sum_m e^{-E_m L_y} |E_m\rangle \langle E_m|$ [139]. Consequently, the 1D quantum ground state energy E_0 dominates in the limit $L_y \gg L_x$ in contributing to the 2D free energy (Shannon entropy of the measurement record) according to $F = E_0 L_y + \dots$. The excitations $E_m - E_0 \propto 2\pi \Delta_m / L_x$ are expected to obey a scaling according to the underlying CFT, and due to the state-operator correspondence, their energy gaps capture certain operator correlation functions in spacetime. We have performed such calculations for the self-dual critical theory for different system sizes, resulting in the ‘‘spectra’’ of Fig. 7, where both Ising and Nishimori criticality are also included for comparison.

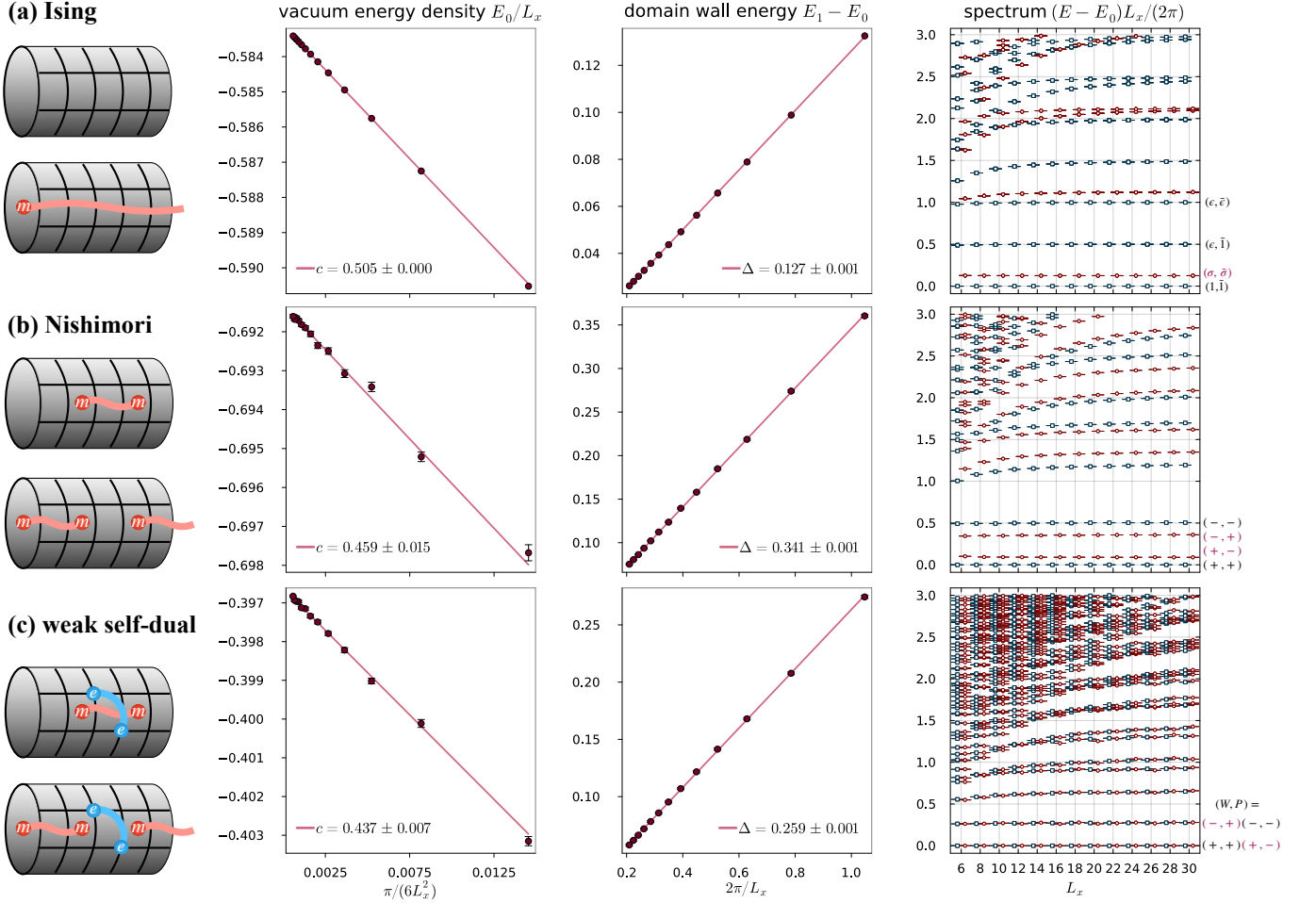


FIG. 7. Numerical computation for the domain wall energy, ground state energy and the Lyapunov spectrum for the many-body states in the second quantization picture, comparing Ising, Nishimori, and weak self-dual critical states. The system size ranges $L_x = 6 \sim 30$. The first column of the data plots lists the vacuum energy density in the even sector. The second column is the domain wall energy, obtained by the energy difference between the ground states of the even sector and the odd sector. The third column is the dimensionless many-body energy or Lyapunov spectrum normalized by the width of the cylinder $L \equiv L_x$. These levels are obtained by filling the energy levels of the single-particle fermion modes in Fig. 5, and they are shifted by a constant such that the ground state level lies at 0. For the spectrum, the black levels with squared markers are for antiperiodic $-WP = -1$ boundary conditions of the fermions, which are composed by the periodic spin chain in the even parity sector $(W, P) = (+, +)$ or the antiperiodic spin chain in the odd parity sector $(W, P) = (-, -)$; the red levels with circle markers include $(W, P) = (+, -)$ and $(W, P) = (-, +)$. The three rows are Ising, Nishimori and weak self-dual, respectively. Here clean Ising is for benchmarking, which exhibits the correct $c = 1/2$ for Casimir energy and $\Delta_{(\sigma, \bar{\sigma})} = 1/8$ for the Ising primary field, and $\Delta_{(\epsilon, \bar{1})} = 1/2$ for the fermion primary field. The sound velocity or the spacetime anisotropy factor is found to be 1 from the clean Ising benchmark, which is consistent with the fact that we work in spacetime isotropic lattice model instead of the continuously weak monitoring limit. For Nishimori we find $E_1 - E_0 \propto 2\pi/L * 0.341(1)$ with sizes up to $L = 30$, which roughly agrees with Merz and Chalker's $\propto 0.691(2)\pi/L$ from the scaling dimension of the vortex-vortex correlation with fermion calculation of sizes up to $L = 22$ [12], and the estimated window in the figures in Ref. [128, 129].

4. Derivation for the noisy Choi state

Choi state as a tensor network state

The noisy state for each trajectory in Eq. (22) is represented by a *bilayer* tensor network state where the noise Kraus operator glues the ket layer and the bra layer, by partially tracing out the e particles. It can be viewed as a “pure” state in the *double* Hilbert space

$$|\rho(e, m)\rangle\rangle = \text{[Diagram of a bilayer tensor network with two layers of tensors and vortices]} = \text{[Diagram of a Choi state tensor } \rho \text{]} \quad (A5)$$

$$\text{---} = \begin{pmatrix} e^{\beta/2} & e^{-\beta/2} \\ e^{-\beta/2} & e^{\beta/2} \end{pmatrix}, \quad \text{---} = \begin{pmatrix} 1 & 1-2p \\ 1-2p & 1 \end{pmatrix}$$

where each bond is a 2-by-2 matrix as written. Again, the e and m vortices inject Pauli Z and X -string to the tensor network. The intra-layer solid bond matrix is the same as above: $[1, e^{-\beta}; e^{-\beta}, 1]$. The dashed bond matrix connecting each site of the ket layer to its counterpart in the bra layer is obtained by tracing out the noise Kraus operations:

$$p \begin{array}{c} \bullet \\ \diagdown \quad \diagup \\ \text{---} \\ \text{---} \\ \bullet \end{array} \begin{array}{c} \text{---} \\ \text{---} \\ \text{---} \\ \text{---} \\ \text{---} \\ \text{---} \\ \bullet \end{array} + (1-p) \begin{array}{c} \bullet \\ \diagdown \quad \diagup \\ \text{---} \\ \text{---} \\ \bullet \end{array} \begin{array}{c} \text{---} \\ \text{---} \\ \text{---} \\ \text{---} \\ \text{---} \\ \text{---} \\ \bullet \end{array} = \begin{array}{c} \bullet \\ \diagdown \quad \diagup \\ \text{---} \\ \text{---} \\ \oplus \\ \text{---} \\ \text{---} \\ \bullet \end{array} \begin{array}{c} \text{---} \\ \text{---} \\ \text{---} \\ \text{---} \\ \text{---} \\ \text{---} \\ \bullet \end{array} \begin{array}{c} \text{---} \\ \text{---} \\ \text{---} \\ \text{---} \\ \text{---} \\ \text{---} \\ \bullet \end{array} \begin{array}{c} \text{---} \\ \text{---} \\ \text{---} \\ \text{---} \\ \text{---} \\ \text{---} \\ \bullet \end{array} \quad (A6)$$

which yields a weight matrix $[1, 1-2p; 1-2p, 1]$ attached to the interlayer dashed bond. With this we can use MPS evolution by MPO to obtain the purity as the norm of the Choi state:

$$\langle\langle \rho(e, m) | \rho(e, m) \rangle\rangle = \text{tr}(\rho^2) = \text{[Diagram of a Choi state tensor } \rho \text{ with its dual } \rho^* \text{]} \quad (A7)$$

Note that this bilayer tensor network also expresses the corresponding classical statistical model - a bilayer interacting Ising model with random e and m disorder. The noise probability tunes the interlayer Ising coupling strength.

Second Rényi coherent information

In the setting for coherent information, one of the physical legs is the reference qubit R , and the second Rényi coherent information (for each trajectory em) is reduced to the logarithm of the expectation of 2 times of the *Bell projector* that

glues the R qubit in the ket and the bra layer

$$I_c^{(2)} = -\ln \text{[Diagram of a Choi state tensor } \rho \text{ with a Bell projector } R \text{ connecting the ket and bra layers]} \quad (A8)$$

evaluated over the *normalized* Choi state (by noting that $e^{-S_{BR}^{(2)}}$ is the purity and thus the norm of the Choi state).

For a more detailed analysis of the contribution of the coherent information, note that the Choi state can be decomposed into 4 states labeled by 2 logical quantum numbers (accounting for the ket and bra space, respectively)

$$|\rho\rangle\rangle_{BR} = \frac{1}{2} \sum_{\mu\nu=\uparrow,\downarrow} |\rho_{\mu\nu}\rangle\rangle_B \otimes |\mu\nu\rangle\rangle_R \quad (A9)$$

The purity is reduced to

$$\text{tr} \rho_{BR}^2 = \frac{\langle\langle \rho_{00} | \rho_{00} \rangle\rangle + \langle\langle \rho_{01} | \rho_{01} \rangle\rangle + \langle\langle \rho_{10} | \rho_{10} \rangle\rangle + \langle\langle \rho_{11} | \rho_{11} \rangle\rangle}{(\text{tr} \rho_{00} + \text{tr} \rho_{11})^2}$$

$$\text{tr} \rho_B^2 = \frac{\langle\langle \rho_{00} | \rho_{00} \rangle\rangle + \langle\langle \rho_{00} | \rho_{11} \rangle\rangle + \langle\langle \rho_{11} | \rho_{00} \rangle\rangle + \langle\langle \rho_{11} | \rho_{11} \rangle\rangle}{(\text{tr} \rho_{00} + \text{tr} \rho_{11})^2} \quad (A10)$$

Therefore, we arrive at the second Rényi coherent information of the noisy state for a fixed em configuration:

$$I_c^{(2)} = S_B^{(2)} - S_{BR}^{(2)} = \ln \frac{\text{tr} \rho_{BR}^2}{\text{tr} \rho_B^2} = -\ln \langle\langle \Pi_R \rangle\rangle$$

$$= \ln \frac{\langle\langle \rho_{00} | \rho_{00} \rangle\rangle + \langle\langle \rho_{01} | \rho_{01} \rangle\rangle + \langle\langle \rho_{10} | \rho_{10} \rangle\rangle + \langle\langle \rho_{11} | \rho_{11} \rangle\rangle}{\langle\langle \rho_{00} | \rho_{00} \rangle\rangle + \langle\langle \rho_{00} | \rho_{11} \rangle\rangle + \langle\langle \rho_{11} | \rho_{00} \rangle\rangle + \langle\langle \rho_{11} | \rho_{11} \rangle\rangle}$$

$$= \ln \frac{\langle\langle \rho_{00} | \rho_{00} \rangle\rangle + \langle\langle \rho_{01} | \rho_{01} \rangle\rangle}{\langle\langle \rho_{00} | \rho_{00} \rangle\rangle + \text{Re} \langle\langle \rho_{00} | \rho_{11} \rangle\rangle} \quad (A11)$$

where in the third line we use the global Ising symmetry and the replica symmetry to reduce half of the terms: $\langle\langle \rho_{00} | \rho_{00} \rangle\rangle = \langle\langle \rho_{11} | \rho_{11} \rangle\rangle$, and $\langle\langle \rho_{\mu\nu} | \rho_{\kappa\eta} \rangle\rangle = \langle\langle \rho_{\nu\mu} | \rho_{\eta\kappa} \rangle\rangle$. The final result depends on only three overlaps of the Choi state in the logical space:

- $\langle\langle \rho_{00} | \rho_{00} \rangle\rangle$ is the vacuum amplitude;
- $\langle\langle \rho_{01} | \rho_{01} \rangle\rangle$ captures the off-diagonal elements of the density matrix of the logical qubit, which suffers from the dephasing error;
- $\langle\langle \rho_{00} | \rho_{11} \rangle\rangle$ describes the bit-flip error for the logical qubit that tunnels the diagonal 0 state to the 1 state.

The four noise scenarios are summarized in Table II below.

Nishimori criticality in the maximally noisy limit

In the maximally noisy limit ($p_s = 50\%$), the records of the e -vortices are destroyed, the decoherence erases the off-diagonal elements from the density matrix leaving only diagonal elements. Concretely, the site indices of the ket and the

TABLE II. Coherent information determined by the logical state density matrix elements.

| logical noise | $ \langle\langle\rho_{01} \rho_{01}\rangle\rangle\rangle$ | $ \langle\langle\rho_{00} \rho_{11}\rangle\rangle\rangle$ | $I_c^{(2)}$ |
|----------------------|---|---|-------------|
| none | 1 | 0 | $\ln 2$ |
| dephase | 0 | 0 | 0 |
| bit-flip | 1 | 1 | 0 |
| bit-flip and dephase | 0 | 1 | $-\ln 2$ |

$|\rho(m)\rangle\rangle =$

 \propto

$$\begin{aligned}
 \text{---} &= \begin{pmatrix} e^\beta & e^{-\beta} \\ e^{-\beta} & e^\beta \end{pmatrix} \\
 \text{---} \triangle &= \begin{pmatrix} \square & \bullet \\ \square & \square \end{pmatrix} \\
 \begin{pmatrix} e^\beta & e^{-\beta} \\ e^{-\beta} & e^\beta \end{pmatrix}^{-\frac{1}{2}} & \begin{pmatrix} e^{\frac{\beta}{2}} & e^{-\frac{\beta}{2}} \\ e^{-\frac{\beta}{2}} & e^{\frac{\beta}{2}} \end{pmatrix}^{\frac{1}{2}} \\
 \text{---} \triangle \text{---} &= \mathbb{I}
 \end{aligned}
 \tag{A12}$$

where the rank-3 triangle tensor at the boundary is the isometry operator, which does not change the entanglement entropy. Therefore we can conclude that our maximally dephased boundary (1+1)D mixed state $|\rho(m)\rangle\rangle$ shares the same entanglement entropy as the (1+1)D Nishimori critical state, falling in the same universality class.

Appendix B: Born-average Rényi entropies

One can generalize Eq. (19) to the Born average of the n -th order Rényi entropies:

$$\frac{1}{1-n} \sum_{em} P(em) \ln \text{tr} \rho_A(em)^n, \tag{B1}$$

which can reveal the multi-fractality of such non-unitary CFT [130] for the same critical point. Note that, in contrast, the Rényi entropies of the mixed state go beyond the Born average and correspond to the higher replica limits described by different critical theories at different critical locations [122]. As shown in Fig. 8, the Rényi entanglement scaling dimensions here clearly deviate from the Calabrese-Cardy formula for unitary CFT, where the central charge is the only fingerprint that governs all the Rényi entanglement entropy. In contrast, here our numerical results show that there are at least two independent exponents $c_{\text{ent}}^{\text{vN}} = 0.795(1)$ and $c_{\text{ent}}^{(\infty)} = 0.484(1)$. From another perspective, given the limited knowledge about

bra layers are locked together, reducing the bulk of the bilayer tensor network into a single layer, except the final time slice. However, the Choi state differs from the (1+1)D boundary MPS of the 2D classical RBIM with Nishimori disorder by only an additional *isometry* tensor that doubles the Hilbert space:

non-unitary CFTs, it is surprising to see that only two parameters are sufficient in describing all the Rényi entropies, which also appear in the case of entanglement transition [145].

Appendix C: Comparison with continuous weak measurement

Here we verify the basic notion of universality - that the critical exponent does not depend on the microscopic details such as spacetime anisotropy, or whether the measurement is discrete or continuous. Namely, the whole self-dual line in Fig. 9 with varying spacetime anisotropy exhibits the same entanglement entropy scaling. To be concrete, we show the entanglement entropy for the weak measurement limit when $\beta \ll 1$ while fixing $\beta' = \beta$, which can be realized from a space anisotropic 2D resource state. In the following we stick to the (1+1)D monitored quantum circuit representation of the problem.

Bimodal discrete weak measurement

Consider weakly measuring an X , the Kraus operator is

$$M_s = \exp\left(\frac{\beta}{2} sX\right) / (2 \cosh \beta), \quad s = \pm 1, \tag{C1}$$

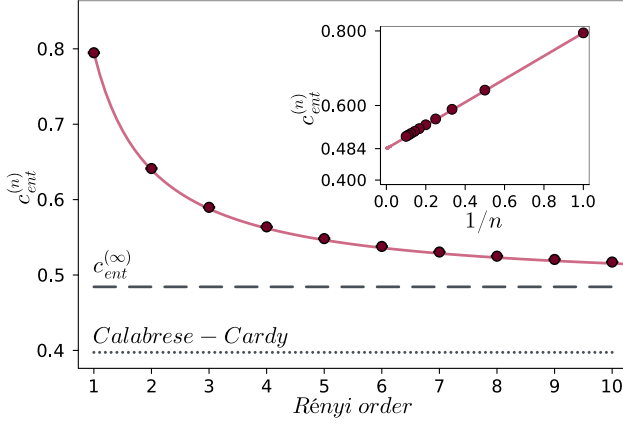


FIG. 8. **Born-average Rényi entropies of the self-dual critical point - their scaling dimensions:** c_n versus Rényi order n . The inset shows that when $n \rightarrow \infty$, $c_{\text{ent}}^{(n)}$ approaches a constant value $c_{\text{ent}}^{(\infty)} = 0.484(1)$. Here the solid line follows the scaling: $c_{\text{ent}}^{(n)} = (c_{\text{ent}}^{\text{VN}} - c_{\text{ent}}^{(\infty)})/n + c_{\text{ent}}^{(\infty)}$, which is should be compared with the Calabrese Cardy formula for unitary CFT $c_{\text{ent}}^{(n)} = c_{\text{ent}}^{\text{VN}}(1+n)/(2n)$. A similar scaling with Rényi indices was observed in the context of measurement-induced phase transitions [145]. The calculation uses parameters $L_x = 512$ and $L_y = 1024$ with periodic spatial boundary conditions, performing 2000 Monte Carlo sweeps using the stochastic fermion evolution method. For L_x ranging from 8 to 32, 1000 Monte Carlo sweeps are performed for the e configuration, conditional upon each of the 500 m configurations.

with probability

$$P(s) = \frac{1}{2 \cosh \beta} \langle \psi | e^{\beta s X} | \psi \rangle = \frac{1 + s \tanh \beta \langle \psi | X | \psi \rangle}{2}, \quad (\text{C2})$$

conditioned upon the state. Check the mean and the variance of this bimodal distribution of the coupling constant to X :

$$\mathbb{E}\left(\frac{\beta}{2}s\right) = \left(\frac{\beta}{2} \tanh \beta\right) \langle X \rangle, \quad \text{Var}\left(\frac{\beta}{2}s\right) = \left(\frac{\beta}{2}\right)^2, \quad (\text{C3})$$

from which we see that $\tanh \beta \in [0, 1]$ expresses the fidelity of the measurement outcome s with the true quantum expectation value $\langle X \rangle$ of the quantum state. Note that at the weak measurement limit $\beta \ll 1$, we have

$$\mathbb{E}\left(\frac{\beta}{2}s\right) = 2\text{Var}\left(\frac{\beta}{2}s\right) \langle X \rangle \quad (\text{C4})$$

One can simply replace X by any other Pauli observables for the equations above. We check that for a small size calculation with very weak measurement strength and highly spacetime anisotropy, the entanglement scaling (Fig. 9b) agrees with $c_{\text{ent}}^{\text{VN}} = 0.795(1)$ as reported for the spacetime isotropic case in the main text, within numerical error bar.

Gaussian continuous weak measurement

Next we consider the continuous weak measurement [103], which turns to the following Kraus operator

$$M(\alpha) = \left(\frac{\gamma dt}{\pi}\right)^{1/4} \exp\left(-\gamma dt \frac{(\alpha - X)^2}{2}\right), \quad \alpha \in (-\infty, +\infty), \quad (\text{C5})$$

with a continuous measurement outcome α , satisfying the normalization condition $\int_{-\infty}^{\infty} M(\alpha) d\alpha = 1$. The Born's rule dictates

$$P(\alpha) = \sqrt{\frac{\gamma dt}{\pi}} \langle \psi | \exp(-\gamma dt (\alpha - X)^2) | \psi \rangle. \quad (\text{C6})$$

In the early derivation of the stochastic Schrödinger equation [102], X was referred to a continuous degree of freedom like the position in space:

$$P(\alpha) = \sqrt{\frac{\gamma dt}{\pi}} \int e^{-\gamma dt (\alpha - x)^2} |\langle x | \psi \rangle|^2 dx.$$

and an approximation was made that the wave function distribution $|\langle x | \psi \rangle|^2$ is much narrower than the Gaussian distribution in such quantum state diffusion, resulting in:

$$P(\alpha) \approx \sqrt{\frac{\gamma dt}{\pi}} \exp(-\gamma dt (\alpha - \langle \psi | X | \psi \rangle)^2),$$

such that the mean and the variance of the coupling constant of X is

$$\mathbb{E}(\alpha \gamma dt) \approx \gamma dt \langle X \rangle, \quad \text{Var}(\alpha \gamma dt) \approx \frac{\gamma dt}{2}. \quad (\text{C7})$$

which also satisfies

$$\mathbb{E}(\alpha \gamma dt) = 2\text{Var}(\alpha \gamma dt) \langle X \rangle, \quad (\text{C8})$$

as physically required for the consistency of the quantum measurement. Using this Gaussian distribution function instead of the bimodal distribution, our numerical computation for a small size (Fig. 9c) does not show significant deviation from 0.795(1) reported for the spacetime isotropic case for size $L_x = 512$.

Appendix D: Central charge of Ising+

Here we discuss the normalization issue of the Ising+ model. In our main text we normalize the probability function of disorder:

$$P(m)' = \frac{\mathcal{Z}(m)^2}{\mathcal{Z}_{\text{Ising}}}, \quad \sum_m P(m)' = 1, \quad (\text{D1})$$

where we denote $\mathcal{Z}_{\text{Ising}} = \sum_m \mathcal{Z}(m)^2$ with Ising coupling constant $\tanh^{-1} \tanh^2 \theta$ as defined in the main text. $\mathcal{Z}(m)^2$ can be represented as a tensor network or a CC network, same as $\mathcal{Z}_{\text{Ising}}$. However, it is *not* straightforward that

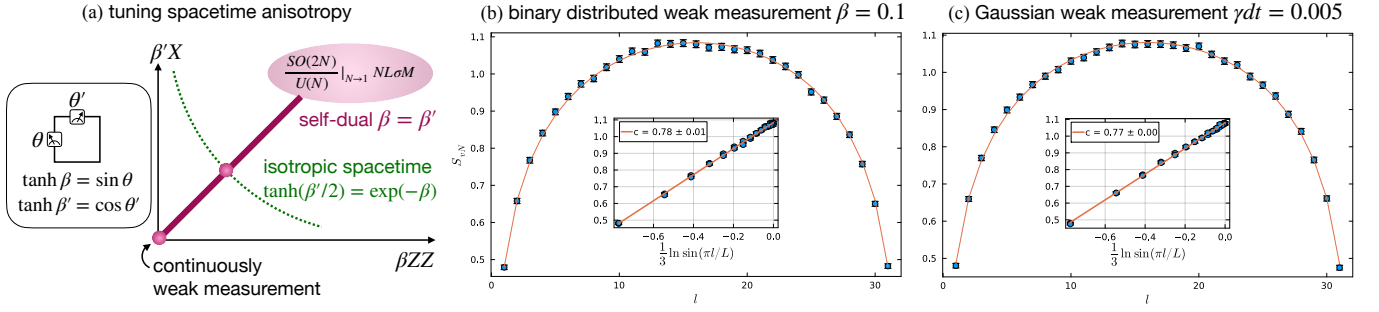


FIG. 9. **Tuning the spacetime anisotropy by varying the measurement strength.** (a) Schematic: the green dashed line corresponds to the spacetime isotropic case we study in the main text, which locks $\beta'/2$ to the KW dual counterpart of $\beta/2$ because we assume a uniform measurement angle θ for the bond qubits in the bulk, which corresponds to an *isotropic* spacetime in the effective statistical model. As shown in the box, if we allow the measurement angle for the horizontal bond qubit θ' to be independently tuned, then we can tune β and β' independently, moving away from the spacetime isotropic line. Then a longer cylinder is needed to reach a steady (1+1)D quantum state. The purple diagonal line $\beta = \beta' < \infty$ respects the self-duality and is expected to flow into the same universality class as described by $SO(2N)/U(N)|_{N \rightarrow 1} NL\sigma M$. (b) Numerical computation for the binary weak measurement $\beta = \beta' = 0.01$ for system size $L_x = 32$, $L_y = 1000$. (c) Numerical computation for the Gaussian weak measurement for system size $L_x = 32$, $L_y = 1000$. Both (b) and (c) roughly agree with that of the finite strength binary measurement $\beta = \ln(1 + \sqrt{2}) \approx 0.8814$ shown in the main text: $c_{\text{ent}}^N \approx 0.795(1)$.

$\mathcal{Z}(m)^2/\mathcal{Z}_{\text{Ising}}$ can be represented as a network, because *inverting a network* - $1/\mathcal{Z}_{\text{Ising}}$ is a highly nonlocal nonlinear operation. In our numerical CC network calculation (as a bilayer tensor network), the transfer matrix generates $\mathcal{Z}(m)^2$ only, without the normalization factor $\mathcal{Z}_{\text{Ising}}$. Therefore the quenched disorder averaged free energy that the Majorana fermion picks up is contributed by two terms:

$$\begin{aligned}
F_{\text{unnorm}} &= - \sum_m P(m)' \ln \mathcal{Z}(m)^2 \\
&= - \sum_m P(m)' \ln [P(m)' \mathcal{Z}_{\text{Ising}}] \\
&= - \sum_m P(m)' \ln P(m)' - \ln \mathcal{Z}_{\text{Ising}} \quad (\text{D2}) \\
&= F_{\text{Ising}+} + F_{\text{Ising}} \\
&= \text{const} \times L_y - \left(c_{\text{Casimir}} + \frac{1}{2} \right) \frac{\pi L_y}{6L_x} + \dots,
\end{aligned}$$

where $F_{\text{Ising}+}$ is the Shannon entropy of the disorder that scales with c_{Casimir} , the effective central charge for Ising+ that we define in this paper. And F_{Ising} is the free energy of the clean Ising model with central charge $1/2$. Therefore, the Majorana fermion sees a combination of c_{Casimir} for Ising+ and $1/2$ from clean Ising. The normalization of the partition function subtracts the $1/2$ contribution.

More generally, for N replicas,

$$\begin{aligned}
F_N \text{ unnorm} &= - \ln \sum_m P(m)'^N \mathcal{Z}_{\text{Ising}}^N \\
&= - \ln \sum_m P(m)'^N - N \ln \mathcal{Z}_{\text{Ising}} \quad (\text{D3}) \\
&= - \ln \sum_m P(m)'^N + N F_{\text{Ising}} \\
&= F_N + N F_{\text{Ising}},
\end{aligned}$$

the unnormalized version of the free energy picks up a background term with the Ising free energy *linearly* coupled to the replica index N . Thus taking the derivative with N yields a replica-independent constant contribution originating from the critical Ising CFT. This is why in our definition the Ising+ has central charge 0 rather than $1/2$: $F_{N=1} = F_{N=1} \text{ unnorm} - F_{\text{Ising}} \propto (1/2 - 1/2) = 0$.

Lyapunov spectrum. Since we do not have a *transfer matrix* for $\mathcal{Z}(m)^2/\mathcal{Z}_{\text{Ising}}$, we cannot define its Lyapunov spectrum. Instead, the Lyapunov spectrum that we compute corresponds to the unnormalized model described by partition function $\mathcal{Z}(m)^2 = \text{tr}(T^{L_y})$, where T is the transfer matrix.

Appendix E: Supplementary data for finite-size data collapse

We close the manuscript by providing supplementary data for the critical states along the three critical line by tuning the e -mass (Fig. 10), e -noise (Fig. 11), and em -mass (Fig. 12), respectively.

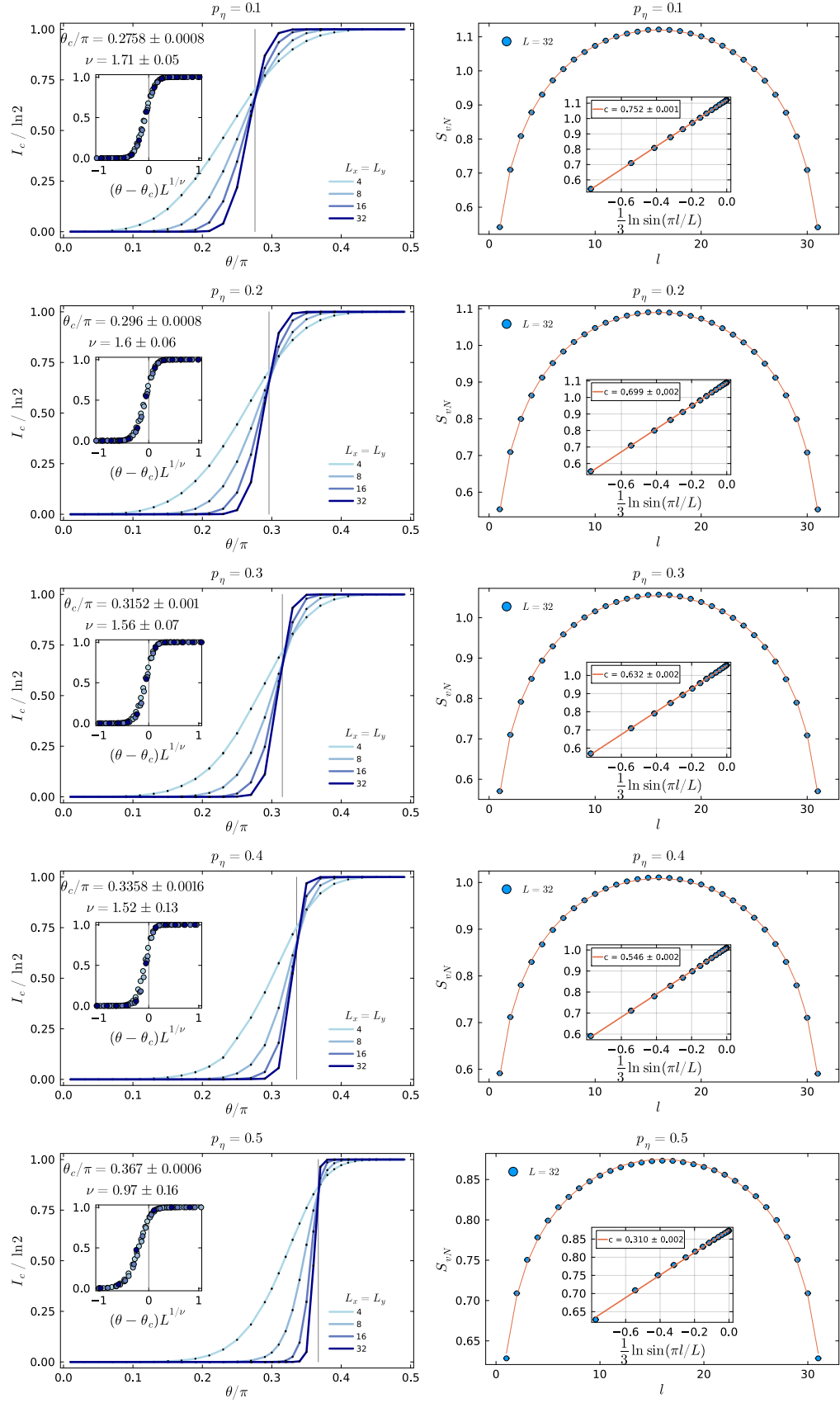


FIG. 10. Phase transitions driven by θ with varying mass of e -vortex: the first column shows the finite size scaling of coherent information signalling the phase transition; the second column shows the Born average bipartite von Neumann entanglement entropies at the critical point.

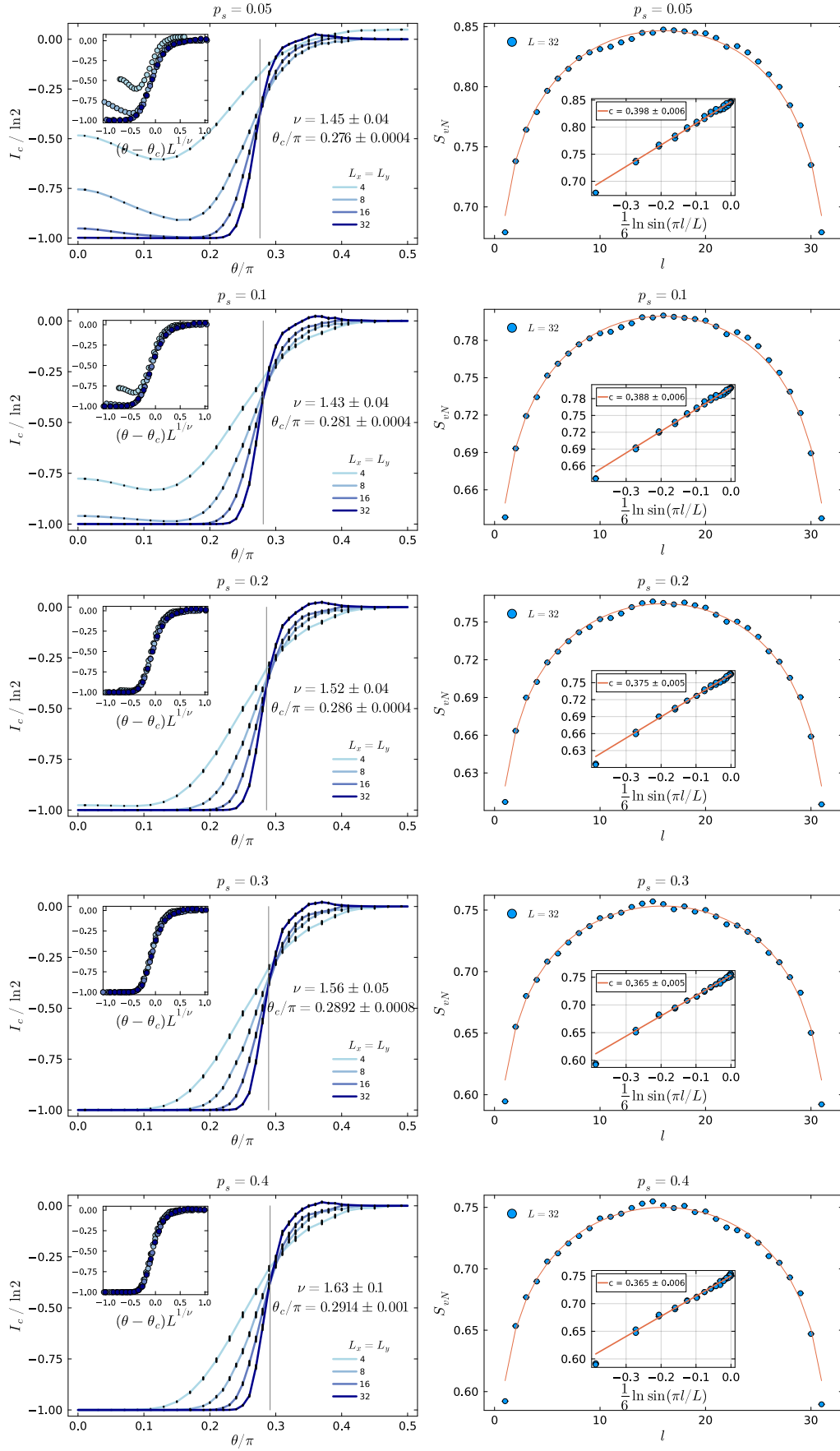


FIG. 11. **Phase transitions driven by θ with varying noise of e -vortex:** the first column shows the finite size scaling of the Born-averaged second Rényi coherent information signalling the phase transition; the second column shows the Born average bipartite von Neumann entanglement entropies of the purified Choi state at the critical point.

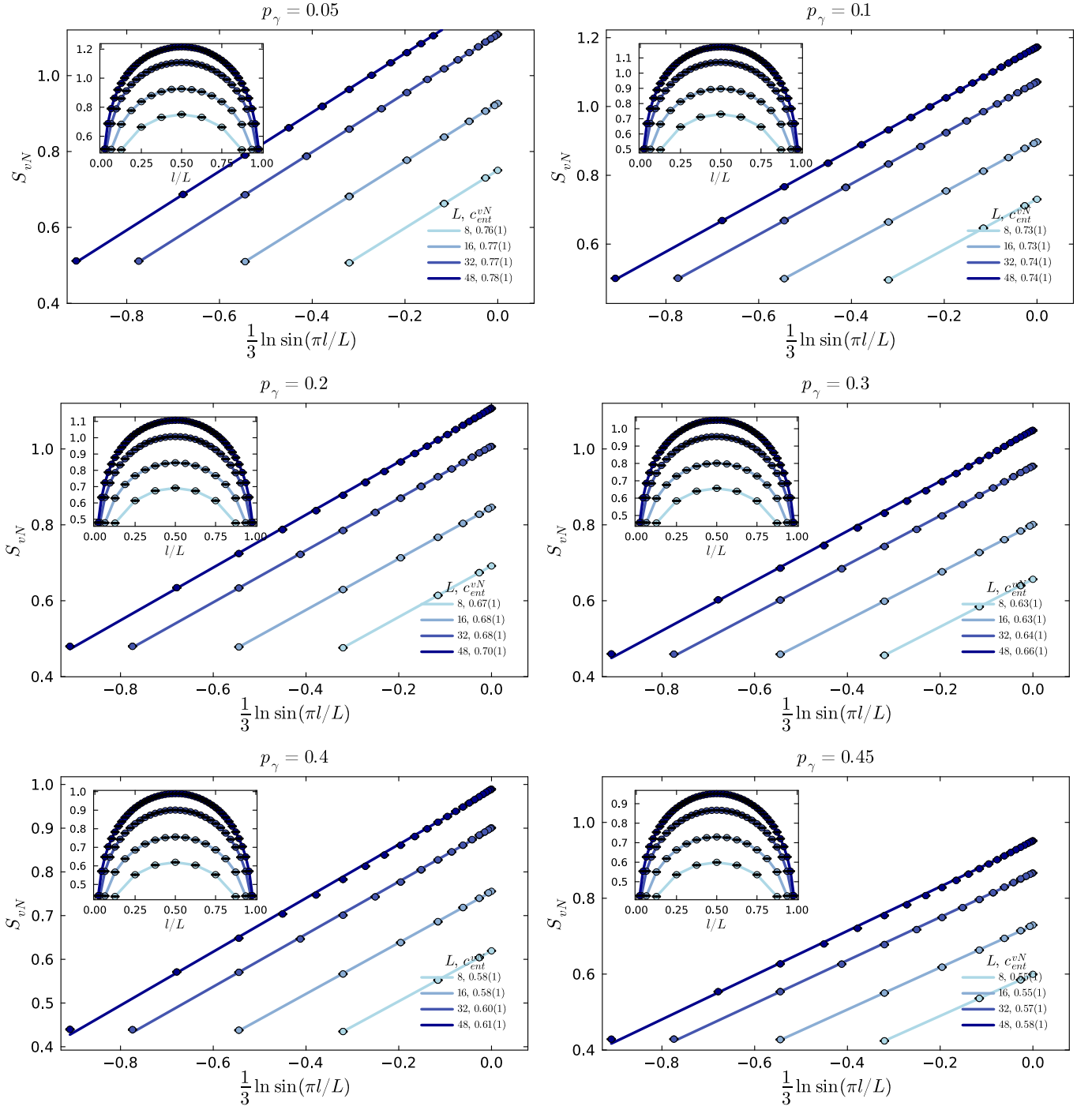


FIG. 12. Von Neumann entanglement entropy scaling for the self-dual mixed state interpolating between weak self-dual and clean Ising by tuning the mass of e and m vortices. The computation is performed at the exactly known self-dual location $\theta = \pi/4$, with Monte Carlo sampling combined with Gaussian fermion evolution.